BRNO UNIVERSITY OF TECHNOLOGY

VYSOKÉ UČENÍ TECHNICKÉ V BRNĚ

FACULTY OF CHEMISTRY

FAKULTA CHEMICKÁ

INSTITUTE OF CHEMISTRY AND TECHNOLOGY OF ENVIRONMENTAL PROTECTION

ÚSTAV CHEMIE A TECHNOLOGIE OCHRANY ŽIVOTNÍHO PROSTŘEDÍ

THERMAL LENS SPECTROMETRIC DETECTION OF MRI CONTRAST AGENTS IN THE PROCESS OF THEIR PHOTOCATALYTIC DEGRADATION

THERMAL LENS SPECTROMETRIC DETECTION OF MRI CONTRAST AGENTS IN THE PROCESS OF THEIR PHOTOCATALYTIC DEGRADATION

MASTER'S THESIS

DIPLOMOVÁ PRÁCE

AUTHOR — **Bc. Michal Petruľák**

AUTOR PRÁCE

SUPERVISOR — **Prof. Dr. Mladen Franko**

VEDOUCÍ PRÁCE

BRNO 2016

Vysoké učení technické v Brně
Fakulta chemická
Purkyňova 464/118, 61200 Brno

Zadání diplomové práce

Číslo diplomové práce:	**FCH-DIP0958/2015**	Akademický rok: **2015/2016**
Ústav:	Ústav chemie a technologie ochrany životního prostředí	
Student(ka):	**Bc. Michal Petruľák**	
Studijní program:	Chemie a technologie ochrany životního prostředí (N2805)	
Studijní obor:	Chemie a technologie ochrany životního prostředí (2805T002)	
Vedoucí práce	**Prof. Dr. Mladen Franko**	
Konzultanti:	doc. Ing. Josef Čáslavský, CSc.	

Název diplomové práce:

Thermal lens spectrometric detection of MRI contrast agents in the process of their photocatalytic degradation

Zadání diplomové práce:

1. Vypracování rešerše z dostupné literatury zaměřené především na: (i) výskyt MRI kontrastních látek v životním prostředí a jejich možné negativní dopady; (ii) způsoby jejich degradace ve vodě; (iii) metody jejich stanovení, a (iv) současný stav Thermal Lens spektrometrie (TLS) použitelné jako detekční metody pro účinnou kapalinovou chromatografii (HPLC), průtokovou injekční analýzu (FIA) a mikroprůtokovou injekční analýzu (uFIA).
2. Optimalizace analytické metody pro stanovení MRI kontrastních činidel pomocí FIA s detekcí TLS. Úprava stávající HPLC metody pro detekci TLS za účelem využitelnosti pro monitorování účinnosti fotokatalytické degradace.
3. Pomocí FIA-TLS, případně systému HPLC-TLS analyzovat vzorky odebrané v procesu fotokatalytické degradace MRI kontrastních činidel ve vodných roztocích.
4. Diskuse dosažených výsledků a jejich porovnání je s publikovanými údaji, zejména účinnost analytické metody, jakož i účinnost fotokatalytické degradace MRI kontraastních látek.

Termín odevzdání diplomové práce: 19.5.2016

Diplomová práce se odevzdává v děkanem stanoveném počtu exemplářů na sekretariát ústavu a v elektronické formě vedoucímu diplomové práce. Toto zadání je přílohou diplomové práce.

Bc. Michal Petruľák Student(ka)	Prof. Dr. Mladen Franko Vedoucí práce	prof. RNDr. Milada Vávrová, CSc. Ředitel ústavu

V Brně, dne 31.1.2016

prof. Ing. Martin Weiter, Ph.D.
Děkan fakulty

ABSTRACT

The Master's thesis are focused on the degradation study of magnetic resonance imaging contrast agents, which are nowadays widely used in the countries with well developed healthcare system. These compounds can be found in the wastewater treatment plans effluent. This indicates, that the conventional water treatment processes are not sufficiently effective in terms of contrast agents removal. Only a little is known about the degradation of gadolinium-based contrast agents. The photocatalytical degradation process and ozonation of chosen compound gadobutrol was followed by: total organic carbon measurements, thermal lens microscopy and spectrophotometry.

ABSTRAKT

Diplomová práce je zaměřena na studium degradace kontrastních látek pro magnetickou rezonanci. Tyto látky se dnes ve velké míře používají v oblastech s rozvinutým zdravotnictvím. Můžeme je najít v odtocích z čistíren odpadních vod, což svědčí o tom, že běžné stupně čištění odpadních vod nejsou dostatečně efektivní pro jejich odstranění. O degradaci kontrastních látek na bázi gadolinia je jen málo informací. Fotokatalytický rozklad za pomoci oxidu titaničitého a také ozonace vybrané kontrastní látky gadobutrolu, byl sledován pomocí měření celkového organického uhlíku, mikroskopie termálních čoček a spektrofotometrie.

KEYWORDS

MRI, contrast agent, gadobutrol, gadolinium, photocatalysis, titanate dioxide, ozonation, AOP, degradation,

KLÍČOVÁ SLOVA

MRI, kontrastní látky, gadobutrol, gadolinium, fotokatalýza, oxid titaničitý, ozonace, AOP, degradace,

PETRUĽÁK, M. *Thermal lens spectrometric detection of MRI contrast agents in the process of their photocatalytic degradation.* Vysoké učení technické v Brně, Fakulta chemická, 2016. 83 s. Vedoucí diplomové práce Prof. Dr. Mladen Franko.

DECLARATION

I declare that the master's thesis has been elaborated by me and that all the quotations from the used literary sources are accurate and complete. The content of master thesis is the property of the Faculty of Chemistry of Brno University of Technology and all commercial uses are allowed only if approved by both the supervisor of thesis and the dean of the Faculty of Chemistry, Brno University of Technology

……

Student's signature

PROHLÁŠENÍ

Prohlašuji, že jsem diplomovou práci vypracoval samostatně a že všechny použité literární zdroje jsem správě a úplně citoval. Bakalářská práce je z hlediska obsahu majetkem Fakulty chemické Vysokého učení technického v Brně (FCH VUT) a může být využita ke komerčním účelům jen se souhlasem vedoucího bakalářské práce a děkana FCH VUT.

……

podpis studenta

ACKNOWLEDGEMENT

Big THANK YOU, to my mentor Prof. Dr. Mladen Franko, for his time, professional approach and guidance.

I am also very thankful to all employees (also former) of the Laboratory for Environmental Research in Nova Gorica which I had a pleasure to meet, for all good suggestions and help, which they provided.

My thanks for useful consultations to doc. Ing. Josef Čáslavský, CSc.

Many thanks also to my collegues from VUT, for thier support and all the good times that we had during the whole study period. – ŽIVKO JEDE!

At last, but not least, my gratitude belongs to my beloved parents Danka & Róbo, for their never-ending support, and also to my girlfriend and other friends for moral encouragements ☺

CONTENT

1. INTRODUCTION

Environmental issues are one of the most serious problems presently faced on the global scale. Pollution and destruction of natural resources are closely connected to industrial growth, development and increasing number of world population. With the introduction of magnetic resonance imaging, many contrast agents for diagnosis quality enhancement have been developed. Every new generation of this agents, has more desirable properties than the previous one. One of the most important aspect is the inertness and high stability of these substances. With the great improvement of healthcare system, an anomaly has emerged 20 years ago in well developed countries. In many rivers, lakes, but also tap water, abnormal quantities of gadolinium have been reported. This metal can have negative effects on human body, especially on the people with renal disfunction. The behavior of Gd chealtes used in magnetic resonance imaging in the process of sewage treatment is widely unknown. Due to the varying toxicity of particular Gd species, it is important not to only investigate the total Gd concentrations, but also the possible degradation methods and mechanisms. These thesis are focused on the degradation of chosen Gd-based contrast assisted by advanced oxidation processes, namely: (i) photocatalysis on the immobilized TiO_2 slides, and (ii) ozonation; which are both promising techniques for wastewater treatment.

2. THEORETICAL PART

2.1 Heterogeneous photocatalysis

2.1.1 Introduction

Interest in TiO_2–based photocatalysis has been noteworthy since Fujishima and Honda's first reports in the early 1970's of UV–induced redox chemistry on TiO_2 [1]. In their more recent report [2] from year 2008, they have published a figure, where we can see dramatical growth of published scientific papers about photocatalysis and photocatalysis with TiO_2 (Fig.1). This high numbers of publications are reflecting the potential of new applications emerging from research in this discipline [3].

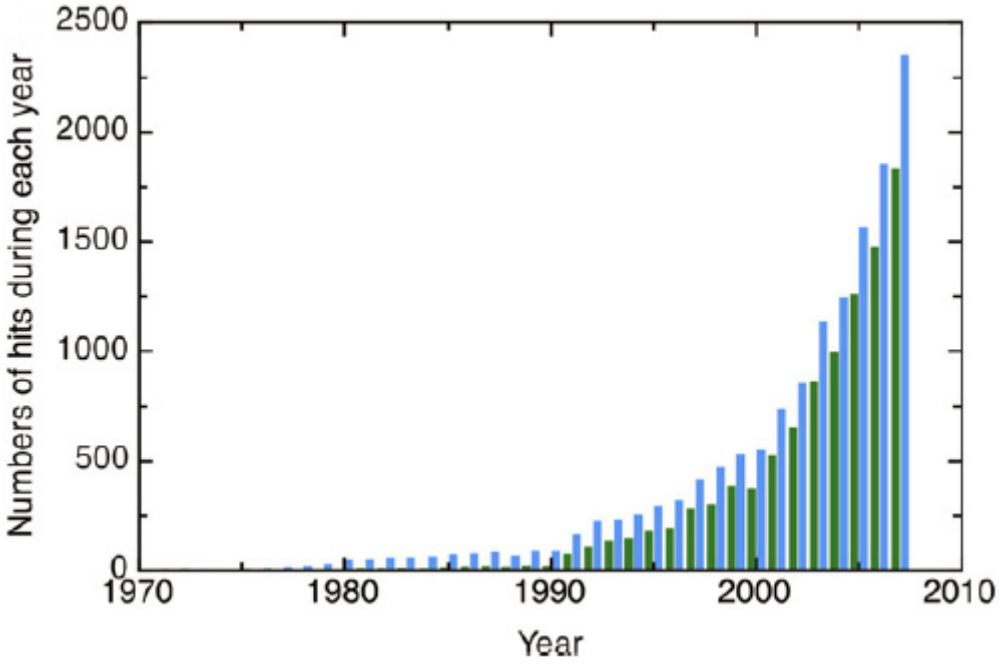

Figure 1. Numbers of research articles appearing on photocatalysis per year: search result in the period of 1972–2007 with the "Web of Science" (a) by the keyword "photocataly*" (blue bars) and (b) the keywords "TiO_2 AND photocataly* " (green bars) [2]

2.1.2 Advanced oxidation processes (AOP's)

Heterogeneous photocatalysis belongs to the group of advanced oxidation processes. These processes can transform organic pollutants into less complex compounds. Ideal scenario is, when the pollutants undergo complete mineralization. AOP's are considered clean technologies for treatment of polluted waters or air and they are based on the concept of producing hydroxyl radicals ($HO^{\bullet}$), which then attack organic pollutants. The efficiency of processes is than

determined by the generation of these highly reactive radicals that are non–selective and powerful oxidizing species (E^0 = 2.80V), which degrade arbitrarily micropollutants with reaction rate constants usually around 10^9 $L.mol^{-1}$ $.s^{-1}$ [4]. Final products are CO_2, H_2O and possibly inorganic ions [5]. The diverse AOP's include following [6]:

1) Photolysis (UV or VUV).
2) Hydrogen peroxide (this includes the H_2O_2 + UV, Fenton: H_2O_2 + Fe^{2+}/Fe^{3+}, Fenton–like reagents: H_2O_2 + Fe^{2+} -solid/Fe^{3+} -solid and photo/Fenton: H_2O_2 + Fe^{2+}/Fe^{3+} + UV).
3) Ozone (ozonation, photo–ozonation, ozonation + catalysis, O_3 + H_2O_2 and O_3 + Fe^{2+}/Fe^{3+}).
4) Photocatalysis (heterogeneous catalysis and photocatalysis and TiO_2 + CdS + combinations).

2.1.3 Photocatalytic materials

Solids that can elevate reactions in the presence of light and are not consumed in the overall reaction are referred to as heterogeneous photocatalysts. These are always semiconductors [7]. An ideal photocatalyst for photocatalytical oxidation is characterized by the following attributes:

- Photo-stability (i.e. not prone to photocorrosion);
- Photo-activity and photo-suitability towards visible or near UV light;
- Chemical and biological inertness;
- Availability and low cost;
- Nontoxicity;
- Capability to adsorb reactants under efficient photonic activation.

Many semiconductors such as TiO_2, ZnO, ZrO_2, CdS, MoS_2, Fe_2O_3, CdS, SnO_2, ZnS, WO_3, etc. have been examined and used as photocatalysts for the degradation of organic compounds. Among them, TiO_2 is the most extensively studied material owing to its properties like resistance towards photocorrosion, availability, non–toxicity, low price and its applicability at ambient conditions [10].

2.1.4 Properties of TiO_2

TiO_2 exists in amorphous form and crystallizes in three different polymorphs in nature according to the order of abundance i.e. rutile, anatase and brookite. As shown in Fig.2, anatase and rutile are tetrahedral while brookite is orthorhombic in structure.

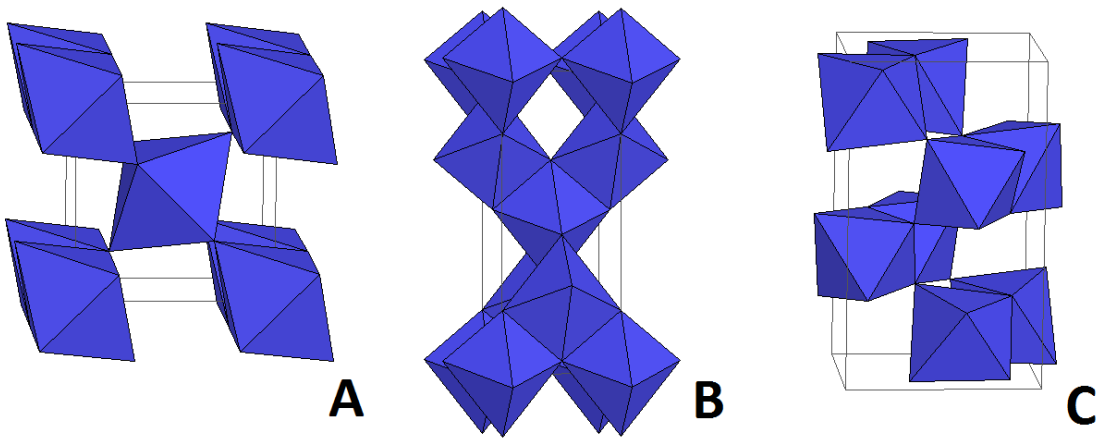

Figure 2. The crystal structures of TiO_2; (a) Rutile, (b) Anatase, (c) Brookite. [8]

Anatase is thermodynamically less stable than rutile and displays a shorter wavelength absorption edge. The structure of rutile and anatase can be described as chains of TiO_6 octahedra. These two crystal structures differ by the distortion of each octahedron and by the assembly pattern of the octahedral chains. On the figure above, we can see unit cell structures of TiO_2 crystals. Each Ti^{4+} ion is surrounded by an octahedron of six O^{2-} ions. The octahedron in rutile is not regular, exhibiting a slight orthorhombic distortion. The octahedron in anatase is significantly distorted so that its symmetry is lower than orthorhombic. The Ti-Ti distances in anatase are greater (3.79 and 3.04 Å versus 3.57 and 2.96 Å in rutile) whereas the Ti-O distances are shorter than in rutile (1.934 and 1.980 Å in anatase versus 1.949 and 1.980 Å in rutile). In the rutile structure each octahedron is in contact with 10 neighbor octahedrons (two sharing edge oxygen pairs and eight sharing corner oxygen atoms). In the anatase structure each octahedron is in contact with eight neighbors (four sharing an edge and four sharing a corner). These differences in lattice structures are causing different mass denseness and electronic band structures [11].

2.1.5 The principles of photocatalysis

Heterogeneous photocatalysis is a discipline consisting of a great variety of reactions like for instance: oxidation, dehydrogenation, metal deposition, hydrogen transfer, photoreduction, disinfection, water detoxification, gaseous pollutant removal, etc. Among them, TiO_2 – assisted heterogeneous photocatalytic oxidation is the main reaction of our interest. Photocatalyst is inducing a series of reductive and oxidative reactions on its surface. This is exclusively conducted by the distinct lone electron feature in its outer orbital. Photocatalytic reaction is induced when the photon energy (*hv*), which is illuminating the semiconductors surface, is higher or equal to its band-gap energy. For TiO_2, it is usually 3.2 eV for anatase and 3.0 eV for rutile. After illumination is the electron photoexcited from the valence band to the empty conduction band in femtoseconds. The mechanisc of the electron–hole pair (e^-–h^+) formation is illustrated on the Fig.3. Adequate photon energy (*hv*) matches with the light wavelengths lower than 380 nm.

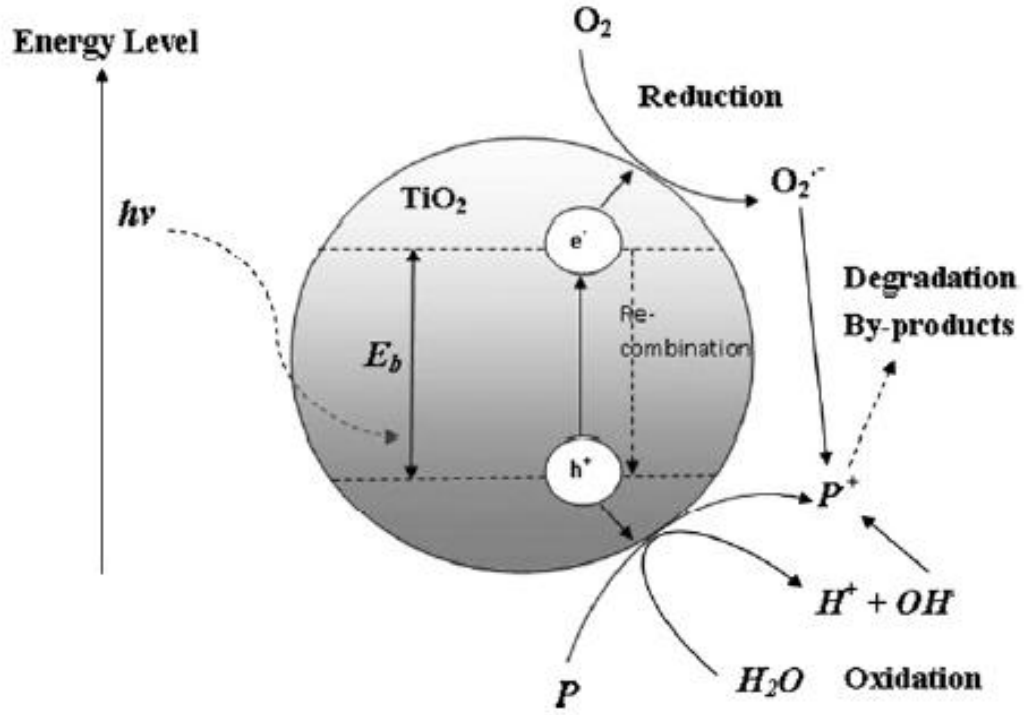

Figure 3. Photo-induced formation mechanism of electron–hole pair in a semiconductor TiO_2 particle with the presence of water pollutant (P). [9]

Creation of (e^{-}–h^{+}) pairs leads to the series of chain oxidative-reductive reactions on the surface as follows:

Photoexcitation:	$TiO_2 + h\nu \rightarrow e^- + h^+$	(1.1)
Charge-carrier trapping of e^-:	$e^-_{CB} \rightarrow e^-_{TR}$	(1.2)
Charge-carrier trapping of h^+:	$h^+_{VB} \rightarrow h^+_{TR}$	(1.3)
Electron-hole recombination:	$e^-_{TR} + h^+_{VB} (h^+_{TR}) \rightarrow e^-_{CB}$ + heat	(1.4)
Photoexcited e^- scavenging:	$(O_2)_{ads} + e^- \rightarrow O_2^{\bullet -}$	(1.5)
Oxidation of hydrolxyls:	$OH^- + h^+ \rightarrow OH^\bullet$	(1.6)
Photodegradation by $OH^\bullet$:	$R–H + OH^\bullet \rightarrow R'^\bullet + H_2O$	(1.7)
Direct photoholes: $R + h^+ \rightarrow R^{+\bullet} \rightarrow$	Intermediate(s)/Final Degradation Products	(1.8)
Protonation of superoxides:	$O_2^{\bullet -} + OH^\bullet \rightarrow HOO^\bullet$	(1.9)
Co-scavenging of e^-:	$HOO^\bullet + e^- \rightarrow HO_2^-$	(1.10)
Formation of H_2O_2:	$HOO^- + H^+ \rightarrow H_2O_2$	(1.11)

The e^-_{TR} and h^+_{TR} (in Eq. 1.4) represents the surface trapped valence band electron and conduction-band hole respectively. It was described [12], that these trapped carriers are usually TiO_2 surface bounded and do not recombine straightaway after photon excitation. When there is a deficiency of electron scavengers (Eq. 1.4), the photoexcited electron recombines with the valence band hole in nanoseconds with simultaneous dissipation of energy in the form of heat. The presence of electron scavengers plays its significant role in prolonging the recombination and hence making the photocatalytical degradation successful. Presence of oxygen (Eq. 1.5) prevents the recombination of electron-hole pair, while allowing the creation of superoxides radicals ($O_2^{\bullet -}$). This $O_2^{\bullet -}$ radical can be further protonated to form the hydroperoxyl radical ($HOO^\bullet$) and afterwards H_2O_2 as shown in (Eqs.1.9 and 1.11), respectively. The $HOO^\bullet$ radical formed was also reported to have scavenging property and thus, the co-existence of these radical species can surely prolong the recombination time of the h^+_{TR} in the entire photocatalysis reaction. It should be noted that we are talking about the systems where dissolved oxygen and water molecules are present. Without water molecules, extremely reactive hydroxyl radicals ($OH^\bullet$) could not be formed and enhance the photodegradation of liquid phase organic pollutants. Nonetheless, some simple organic molecules (e.g. oxalate and formic acid) can be mineralized by direct electrochemical oxidation where the e^-_{TR} is scavenged by metals ions in the systems without water [13]. Many mechanistic studies aimed on different organic compounds have been carried out. Aromatic compounds can be hydroxylated by the reactive $OH^\bullet$ radical, which leads

to successive oxidation and potentially ring opening. The resulting intermediate products consist mostly from aldehydes and carboxylic acids. These are afterwards further carboxylated into carbon dioxide and water. The whole process than can be summarized as follows [9]:

$$\text{Organic Contaminants} \rightarrow \text{Intermediate(s)} \rightarrow CO_2 + H_2O \qquad (1.12)$$

2.1.6 Reaction kinetics

The overall reaction (Eq. 1.12) can be splitted into five independent steps, illustrated in Fig.4 [14]:

1. Mass transport of the organic contaminant(s) (e.g. A) in the liquid phase to the TiO_2 surface.
2. Adsorption of the organic contaminant(s) onto the photon activated TiO_2 surface (i.e. surface activation by photon energy occurs simultaneously in this step).
3. Photocatalytical reaction of the adsorbed phase on the TiO_2 surface (e.g. A→ B).
4. Deposition of intermediate(s) (e.g. B) from the TiO_2 surface.
5. Mass transfer of the intermediate(s) (e.g. B) from the interface area to the bulk fluid.

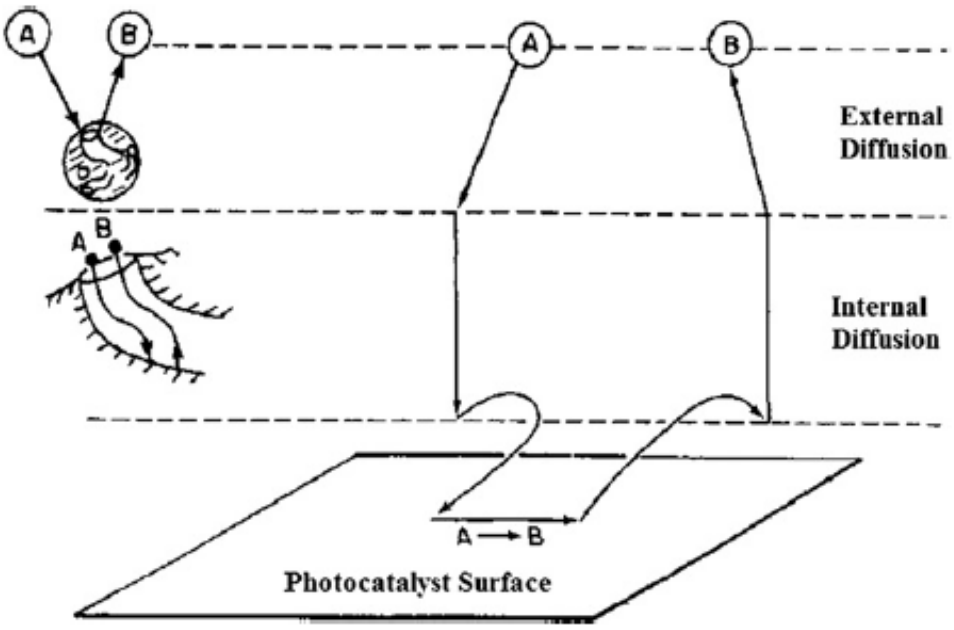

Figure 4. Steps in heterogeneous catalytic reaction [14].

The overall rate of the reaction is equal to the slowest pace. When the mass transfer steps (1 and 5) are very fast compared to the rest of reaction steps (2, 3 and 4), the organic concentrations in the immediate neighborhood of the active sites are identical to those in the bulk liquid phase. In this case, the mass transfer steps are not rate limiting and do not have impact on

the overall rate of photocatalytic reaction. Photodegradation rate is dependent on pollutant's surface coverage of the utilized photocatalysts [15]. This fact highlights the importance of molecules adsorption onto surface and the surface contact with the catalyst during the photocatalytic degradation. If the mass transfer steps are suppressed, a change in the aeration or liquid flow conditions over the TiO_2 photocatalyst may alter the overall photocatalytic reaction rate. Same rule applies for the photo-disinfection. The surface interaction between microorganisms and catalyst is essential for effective disinfection process [14].

2.1.7 Influence of various parameters governing the kinetics

2.1.7.1 Mass of catalyst

The initial reaction rates are directly related to the mass *m* of catalyst. Nevertheless, when the mass is larger than certain value, the rate of reaction becomes independent of *m*. This limit is depending on the geometry and on the working conditions of the photoreactor. These limits are corresponding to the maximal amount of TiO_2 in which all the particles - i.e. all the surface exposed – are entirely irradiated. If the amounts of catalyst are too high, hindering effect takes place – i.e. photosensitive surface is partly masked by the excess mass of catalyst. Optimal mass of photocatalyst must be chosen in order (i) to avoid useless excess of catalyst and (ii) to be sure, that the absorption of efficient photons is maximal. These values usually range from 0.2 g/L to 2.5 g/L of titanium in slurry batch photoreactors [16].

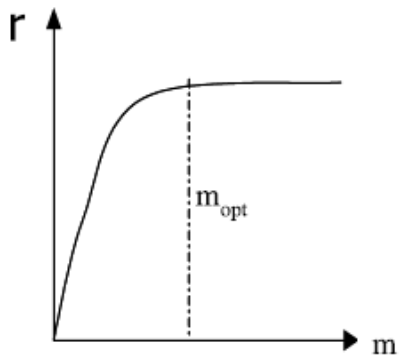

Figure 4. Influence of catalyst mass *m* on the photocatalytic reaction rate *r*. [16]

2.1.7.2 Wavelength

Reaction rate as a function of the wavelength follows the absorption spectrum of the catalyst, with a threshold corresponding to its band-gap energy. For TiO_2 having band-gap energy 3.2 eV for anatase and 3.0 eV for rutile it requires: $\lambda \leq 400$ nm and $\lambda \leq 380$ nm respectively, i.e. near-UV wavelengths (UV-A). It is also crucial, that the reactants do not absorb the light to preserve the photoactivation of the catalyst for a true heterogeneous catalytic process (no homogeneous or photochemistry in the absorbed phase). Photocatalysis can be also triggered by the sun radiation (i.e. Helio-photocatalysis), since it contains about 3-5% of UV-energy [16].

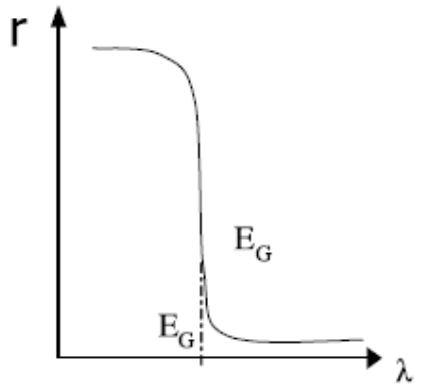

Figure 5. Influence of wavelength λ on photocatalytic reaction rate r. [16]

2.1.7.3 Initial concentration

The kinetics follows a Langmuir-Hinshelwood mechanism endorsing the heterogeneous catalytic nature of the system with the rate r varying proportionally with the coverage θ as:

$$r = k\theta = k\big(KC/(1+KC)\big) \qquad (2.1)$$

Where k is the true rate constant; K is the constant of adsorption at equilibrium and C is the instantaneous concentration.

For the low concentration solutions $(C < 10^{-3}\ M), KC$ becomes $\ll 1$ and the reaction is of the apparent first order, whereas for concentrations $> 5 \times 10^{-3}\ M, (KC \gg 1)$, the reaction rate is maximal and is of the apparent order.

In the gas phase, alike Langmuir-Hinshelwood expressions have been found including partial pressures P instead of C. In some instances, such as liquid alcohol dehydrogenation [17], the rate follows variations including the square root of concentration:

$$r = k\left[K^{1/2}\,C^{1/2} \,/\, \left(1 + K^{1/2}\,C^{1/2}\right)\right] \qquad (2.2)$$

This manifests that the active form of the reactant is in a dissociated adsorbed state. In other cases, a zero kinetic order was found, even at low concentrations. This was caused by the chemisorptions. For a maximum yield, reactions should be performed with initial concentrations equal to, or higher that the threshold of the plateau $(C_0 \geq ca.5 \times 10^{-3}M)$ [16].

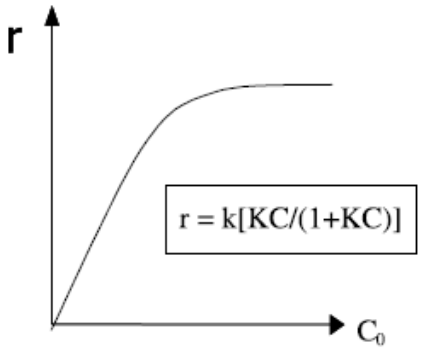

Figure 6. Influence of initial concentration C_0 on photocatalytic reaction rate r. [16]

2.1.7.4 Temperature

Photocatalytic reactions are triggered by photons. This means that no heating is needed, and they are thus operational at ambient temperatures. The true activation energy E_t, relative to the true rate constant k $\left(k = k_0^{\left(-E_c/RT\right)}\right)$, is zero, whereas the apparent activation energy E_a is often very small in the medium temperature range $(20°C \leq \theta \leq 80°C)$. Nonetheless, at very low temperatures $(-40°C \leq \theta \leq 0°C)$, the activity is reduced and the activation energy E_a becomes positive. At higher temperatures $(\theta°C \geq 70 - 80°C)$ for various types of photocatalytic reactions, the activity decreases and the apparent activation energy becomes negative [16].

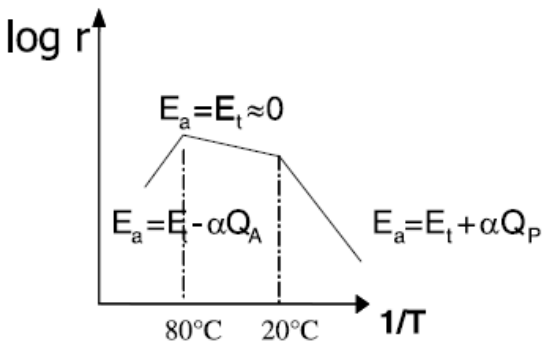

Figure 7 Influence of temperature *T,* on photocatalytic reaction rate r. [16]

2.1.7.5 Radiant flux

The reaction rate of photocatalytic reactions *r* is greatly depending on the radiant flux Φ. This is due to photo-induced character of the activation process, with the participation of photo-induced electrical charges (i.e. electrons and holes) in the reaction mechanism. However, above certain value, which was estimated in laboratory experiments to be around 25 m.W/cm^2, the reaction rate *r* becomes proportional to $\Phi^{1/2}$. This is due to the rate of electron-hole formation, which becomes greater than the photocatalytic rate. In any photocatalytic device, the optimal light power usage corresponds to the domain where *r* is proportional to Φ [16].

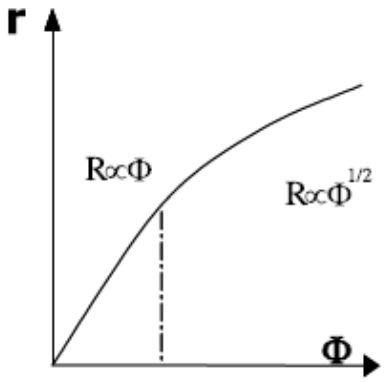

Figure 8. Influence of the radiant flux Φ on photocatalytic reaction rate r. [16]

2.1.7.6 The pH

The pH plays multiple roles in the process of photocatalytical degradation. First, it is related to the ionization state of the surface according to the following reactions:

$$TiOH + H^+ \rightleftharpoons TiOH_2^+ \qquad (2.3)$$

$$TiOH + OH^- \rightleftharpoons TiO^- + H_2O \qquad (2.4)$$

The pH change can thus have influence on the contaminant adsorption onto surface of the photocatalyst. This process is very important for the photocatalytic oxidation to take place [18]. Acid-base properties of the metal oxide surfaces can have considerable implications upon their photocatalytic activity. The point of zero charge of the TiO_2 (Degussa P25) is at pH 6.8 [19]. Thus, the TiO_2 surface is positively charged in acidic media (pH < 6.8), whereas it is negatively charged under alkaline conditions (pH > 6.8).

Second, hydroxyl radicals can be formed by the reaction between hydroxyl ions and positive holes (eq.1.6). The positive holes are considered as the major oxidation species at low pH whereas hydroxyl radicals are considered as the pre-dominant species at neutral or high pH levels [20].

Third, the TiO_2 particles tend to agglomerate under acidic conditions and the surface area available for contaminant adsorption and photon absorption would be reduced [21].

2.1.7.7 Electron Scavengers

Electron scavengers play an important role by obstructing electron-hole recombination. Oxygen acts efficiently as an electron scavenger, preventing the recombination of photo-generated electrons and holes. When amount of oxygen is limited, the fast recombination of electrons and hole in TiO_2 would greatly reduce its photocatalytic effectivity. In lack of oxygen, inorganic oxidants such as IO_4^-, $S_2O_8^{2-}$, BrO_3^-, ClO_3^-, and H_2O_2 can scavenge the conduction-band electrons and form reactive radical intermediates, hence reducing the probability of recombination of the photo-generated electrons and holes. This leads to enhancement of pollutant photodegradation by valence holes [22-24]. However, the relative efficiency of these oxidants has not been reported as it varies from system to system [7].

2.1.7.8 Oxygen

Molecular dissolved oxygen is an efficient electron scavenger and forms $O_2^{\cdot-}$. Molecules of oxygen on the catalyst surface are providing a natural drain for the photo-generated electrons. The $O_2^{\cdot-}$ formed, may generate hydrogen peroxide (eq.1.9-1.11). The generated hydrogen peroxide, may than undergo photo-induced degradation, mainly on the surface of the catalyst, by direct interaction with photo-generated charged species, i.e. h_{VB}^+, e_{CB}^-, or other reactive species such as hydroxyl radicals or superoxide radical anion [7].

2.1.7.9 Hydrogen peroxide

Hydrogen peroxide can likewise oxygen enhance the photocatalytic oxidation process. It can actually entrap e_{CB}^- even more efficiently. During the reaction, hydrogen peroxide also produces $HO^{\cdot}$ by reacting with $O_2^{\cdot-}$ or by direct photolysis (eq. 2.5; 2.6). Nevertheless, when present at high concentration, it renders an inhibition of photocatalytic oxidation process due to scavenging

of h_{VB}^{+}, and $HO^{\cdot}$ [25] (eq. 2.7; 2.8; 2.9). Besides this, H_2O_2 can be adsorbed onto TiO_2 particles to modify their surfaces and after decrease their catalytic activity [7].

$$H_2O_2 + O_2^{\cdot -} \rightarrow HO^{\cdot} + HO^{-} + O_2 \quad (2.5)$$

$$H_2O_2 + h\nu \rightarrow 2HO^{\cdot} \quad (2.6)$$

$$H_2O_2 + 2h_{VB}^{+} \rightarrow O_2 + 2H^{+} \quad (2.7)$$

$$H_2O_2 + HO^{\cdot} \rightarrow H_2O + HO_2^{\cdot} \quad (2.8)$$

$$HO_2^{\cdot} + OH^{\cdot} \rightarrow H_2O + O_2 \quad (2.9)$$

2.1.7.10 Peroxydisulphate

The presence of the oxidant peroxydisulphate ($S_2O_8^{2-}$, e.g. $K_2S_2O_8$) can similarly as above mentioned scavengers, accelerate the photocatalytic process by ensnaring conduction-bad electrons and thereafter prevent its recombination with holes. At the same time, it produces $SO_4^{\cdot -}$, a very strong oxidant (E^0 = 2.5-3.1 V) [25] (eq. 2.10). An important feature of using $S_2O_8^{2-}$ as e_{CB}^{-} scavenger is, that it produces $HO^{\cdot}$ radicals in aqueous solution at various pH values (eq. 2.11). In fact, $SO_4^{\cdot -}$ starts decomposing into $HO^{\cdot}$ at pH>8.5, and $HO^{\cdot}$ becomes the major species at pH>10.7 [26].

$$S_2O_8^{2-} + e_{CB}^{-} \rightarrow SO_4^{2-} + SO_4^{\cdot -} \quad (2.10)$$

$$SO_4^{\cdot -} + H_2O \rightarrow SO_4^{2-} + HO^{\cdot} + H^{+} \quad (2.11)$$

2.1.7.11 Periodates

Periodate ion has more than two atoms of oxygen per one halogen atom, where I is the central atom. Polarizability variations in the constituent atoms of IO_4^{-} , can capture conduction-band electrons (eq. 2.12) generated by photocatalyst more efficiently than other oxidants. Besides trapping of conduction-band electrons, periodate undergoes decomposition under UV light and generates numerous highly reactive radicals (eq. 2.13; 2.14) and nonradical intermediates [27-29] including $HO^{\cdot}$. It was reported that the reaction rate order with respect to periodate is 0.8 times higher than that for hydrogen peroxide [30]. The fact that IO_4^{-} is a more effective oxidant than $S_2O_8^{2-}$ and H_2O_2 for degradation, has been reported in some studies. However, the concentration of IO_4^{-} must be optimized, due to hydroxyl radicals scavenging at higher concentrations (eq.2.15) [7].

$$IO_4^- + 8e_{CB}^- + 8H^+ \rightarrow 4H_2O + I^- \quad (2.12)$$

$$IO_4^- + hv \rightarrow IO_3^{\cdot -} + O^{\cdot -} \quad (2.13)$$

$$O^{\cdot -} + H^+ \rightleftharpoons HO^{\cdot} \quad (2.14)$$

$$HO^{\cdot} + IO_4^- \rightarrow HO^- + IO_4^{\cdot} \quad (2.15)$$

2.1.8 Application

2.1.8.1 Environment

Due to the unique photocatalytic and photo-induced superhydrophilic properties, TiO_2 is potentially useful in three major areas of environmental applications: (i) production of self-cleaning surfaces [30], (ii) degradation of volatile organic/inorganic compounds in the gas phase [31-33], and (iii) waste water treatment [34-36] and disinfection of drinking water [37-39]. Photocatalytic reactors used for water treatment can be classified according to either those with an immobilized photocatalyst or with the photocatalyst suspended in the aqueous medium. There are several types of photocatalytic reactors [40] with immobilized TiO_2 and among them, packed-bed and monolith photocatalytic reactors are offering remarkable advantages: (i) no post-separation process is needed, (ii) the photocatalytic surface can be significantly increased by using the proper substrate (e.g. glass beads, fibers, foamed ceramics), (iii) these substrates or fillers enhance the mixing of reactants, which tends to reduce undesirable diffusive resistances, and (iv) these two types of photocatalytic reactors have less catalyst attrition problems than the fluidized bed reactors [41].

2.1.8.2 Construction materials

The usage of TiO_2 in construction materials, is the highest among all TiO_2 applications on the market [42]. This is because of TiO_2 photo-induced superhydrophilicity. Superhydrophilic properties are acquired after UV illumination. In this case, electrons and holes are still produced, but they react in a different way. The electrons tend to reduce Ti(IV) cations to the Ti(III) state, and the holes may oxidize the O^{2-} anions. In the process, oxygen atoms are ejected, creating oxygen vacancies. Water molecules can then occupy the oxygen vacancies, producing absorbed OH groups, which tend to make the surface hydrophilic. The longer the surface is illuminated with UV light, the smaller the contact angle for water becomes. After about half an hour under moderate UV light intensity, the contact angle approaches zero, meaning that water has tendency to spread completely across the surface [43]. This surface phenomenon of anti-fogging properties

is used for various kind of purposes e.g. road mirrors, mirrors for bathrooms, heat exchangers, glass films, windshields, optical and contact lenses.

The combination of photocatalytic and superhydrophilic properties is perfect for the outdoor self-cleaning materials e.g. glass, tiles, tents, plastic films, aluminum panels, coatings and particularly for road-construction materials with the air cleaning properties e.g. soundproof walls, tunnel walls, road-blocks, coatings, traffic signs and reflectors, lamp covers [44].

2.1.8.3 Self-sterilizing surfaces

As was mentioned before, TiO_2 photocatalysis can be used to kill bacteria. This is profitable not only in waste/drinking water treatment, but also for the self-sterilizing surfaces. The first experiments were carried out with *E. coli* suspensions [45]. A typical experiment involves placing bacteria suspension containing $3x10^4$ cells on an illuminated TiO_2-coated glass plate (1 m.W.cm^{-2} UV light). Under these conditions, there were no surviving cells after only 1 hour of illumination. By contrast, after 4h under UV illumination without a TiO_2 film, only 50% of the cells were killed. Nowadays, this can be used for places with high hygienic standards i.e. hospitals, where its suitable to use for floor/wall tiles of operating rooms, silicone rubber for medical catheters or hospital garments and uniforms. It is also suitable for use in the public rest rooms and bathrooms [43, 44]. There are a lot of patents containing claims or information related to photocatalytic disinfection or cell killing (Tab.1; Tab.2) [46].

2.2 Magnetic resonance contrast agents

2.2.1 Magnetic resonance

Magnetic resonance imaging (MRI) is a powerful medicinal imaging modality to display anatomical structures of body, especially used for the detection and characterization of diseased soft tissues, e.g. solid tumors. MRI has many advantages as it has no ionizing radiation and provides three-dimensional images with high spatial resolution and high contrast. In the last 30 years, the quality of MR body images, including spatial resolution, signal-to-noise and contrast-to-noise ratios, has been greatly improved. In addition to stronger magnets, the development of effective and safe contrast agents (CA) has played an important role for improving the scan image quality by enhancing the image contrast between normal and diseased tissues [47].

2.2.2 Magnetic resonance contrast agents

Magnetic resonance contrast agents are biocompatible magnetic materials that alter the longitudinal (T_1) and transverse (T_2) relaxation rates of the surrounding water protons, therefore enhancing image contrast in tissues of interest [48]. MRI contrast agents are generally categorized as T_1 and T_2 CA based on their magnetic properties and relaxation mechanisms. Gadolinium Gd(III) chelates are effective for increasing T_1 relaxation rate ($1/T_1$) and commonly used as a T_1 CA, generating a positive image contrast. Superparamagnetic iron oxide nanoparticles are more effective for increasing T_2 relaxation rate ($1/T_2$) and commonly used as T_2 CA. producing negative image contrast. The majority of MRI CA used in clinical practice are Gd(III) chelates, with over 10 million contrast enhanced MRI scans on an annual basis, because of their high paramagnetism, favourable properties in terms of relaxation enhancement, relatively high stability and inertness in the body [49].

From the viewpoint of clinical applications, clinical contrast agents can be divided into two main categories: (i) positive, i.e. extracellular agents, blood pool agents and hepatobiliary agents, and (ii) negative, i.e. passive targeting and blood-pool imaging [52]. Those with a wide clinical application can be classified as extracellular, blood pool, and hepatobiliary agents, as well as pharmaceuticals enhancing the lymph nodes, liver and tumors [51].

Since the observation of difference in the nuclear magnetic relaxation times of normal tissues and tumors, MRI has played a significant role in cancer prediction and diagnosis [50]. Paramagnetic CA have been utilized to enhance the image contrast for more accurate cancer detection and diagnosis, and timely evaluation of therapeutic efficiency [47]. About 35% of MRI examinations involve the use of contrast agent (by the year 2013), but this percentage is expected to increase further following the development of more effective and specific contrast media [51].

2.2.2.1 Gd-based contrast agents

Gd-based CA belongs to the T_1 group of agents with longitudinal relaxation. In this category we can find also other paramagnetic ions, specifically transition metals and lanthanide metals with unpaired spins, but for the metal to be effective as a relaxation agent, the electron spin-relaxation time must match the Larmor frequency of the protons. This condition is met better for the Fe^{3+}, Mn^{2+}, and Gd^{3+} ions. We can find also some other paramagnetic metals in the Table 1 [53].

Table 1. Some of the paramagnetic metal ions[53]

Ion	Configuration	Magnetic moment
$^{24}Cr^{3+}$		3.9
$^{25}Mn^{2+}$		5.9
$^{26}Fe^{3+}$		5.9
$^{29}Cu^{2+}$		1.7
$^{63}Eu^{3+}$		3.4
$^{64}Gd^{3+}$		7.9
$^{66}Dy^{3+}$		10.6

Gadolinium, a representative of the rare earth elements (REE), is the most commonly used metal. Unfortunately, Gd^{3+} is highly toxic and shown to inhibit Ca^{2+} binding. Acute toxicity of Gd^{3+} can cause ataxia, writhing, respiratory problems, sedation, hypotension, and death by cardiovascular collapse. Therefore, Gd in MRI techniques is applied as a very stable chelate complex [54]. The ideal chelator prevents interactions between Gd^{3+} ions and endogenous tissues, and thus allows rapid renal excretion of the complex without significant biotransformation or accumulation in the body. Polyaminocarboxylic acids are the most common molecular group in these water soluble agents. Two categories of gadolinium based CA are currently in use: (i) macrocyclic chelates where Gd is “caged” in a pre-organized cavity of the polyaminopolycarboxylic ligand, namely: Gd-DOTA and Gd-BT-DO3A, and (ii) “open-chain” or “linear” chelates, such as Gd-DTPA and Gd-BOPTA. The second type of classification is based on ionic and non-ionic properties. The structure of most common Gd-based contrast agents can be seen on the Fig.10 and Fig.11. [55].

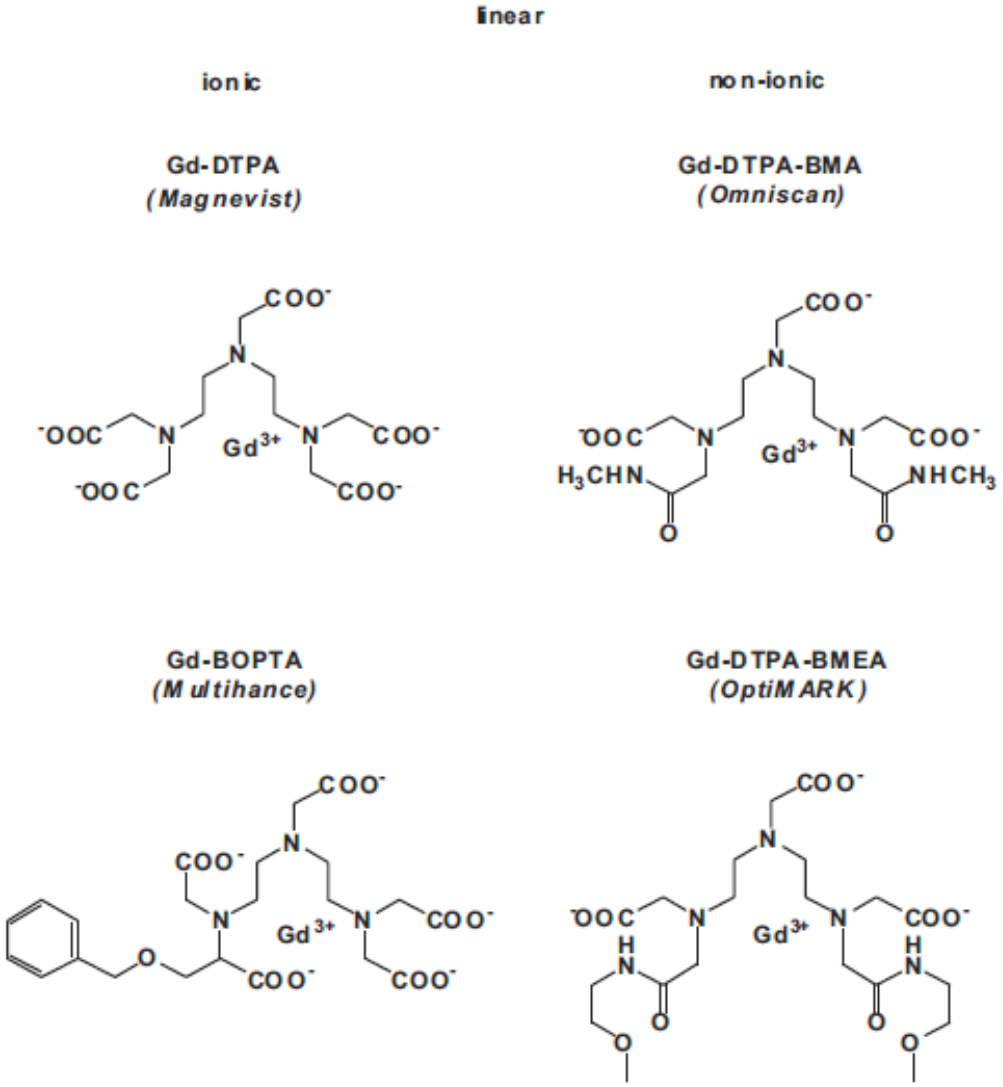

Figure 10. Structures of several linear Gd-based MRI contrast agents and the representative trademarks [56].

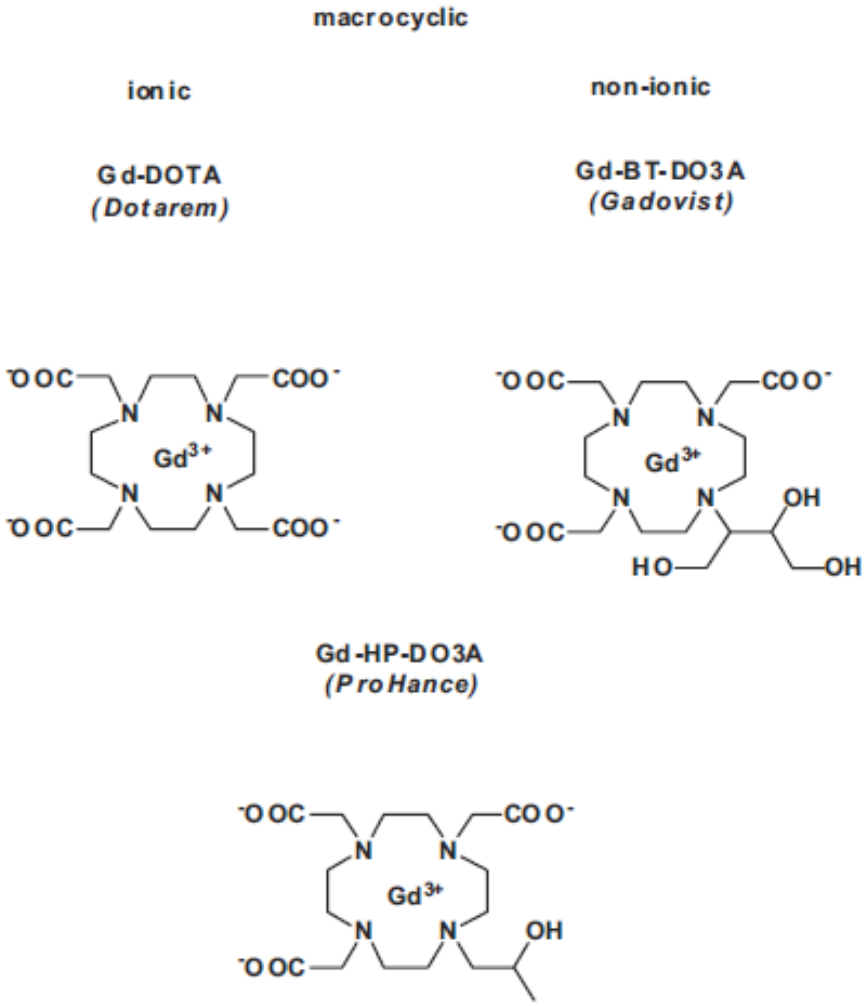

Figure 11. Structures of several macrocyclic Gd-based MRI contrast agents and the representative trademarks [56].

2.2.3 Gadolinium chelates in environment

In general, Gd-based MRI contrast agents are stable complexes. After admission by patients, they are rapidly eliminated from the patient's body. After excretion, they enter the public sewer and after the waste-water treatment plant (WWTP). These treatment plants are designed to remove toxic matter, contaminants and also pharmaceuticals. Owing to their polar or anionic nature, the Gd complexes are most likely neither adsorbed onto surfaces nor by particulate organic matter. Studies of the past decade indicated that sewage treatment leaves the Gd chelates almost unaffected [56, 57].

2.2.3.1 Anthropogenic gadolinium in wastewater and surface waters

In 1996, Bau and Dulski published observations of large positive Gd anomalies in several environmental water samples [58]. In this extensive study, 21 different rivers, tap water in Berlin, surface water of the Baltic Sea, the effluent of a wastewater treatment plant and hospital were sampled. Analysis of all rare earth elements (REE) was done simultaneously by ICP-MS. REE concentrations varied over two orders of magnitude between the different samples. The normalized REE patterns displayed positive Gd anomalies. The anomaly ratios ranged in between 1.5 and 240.

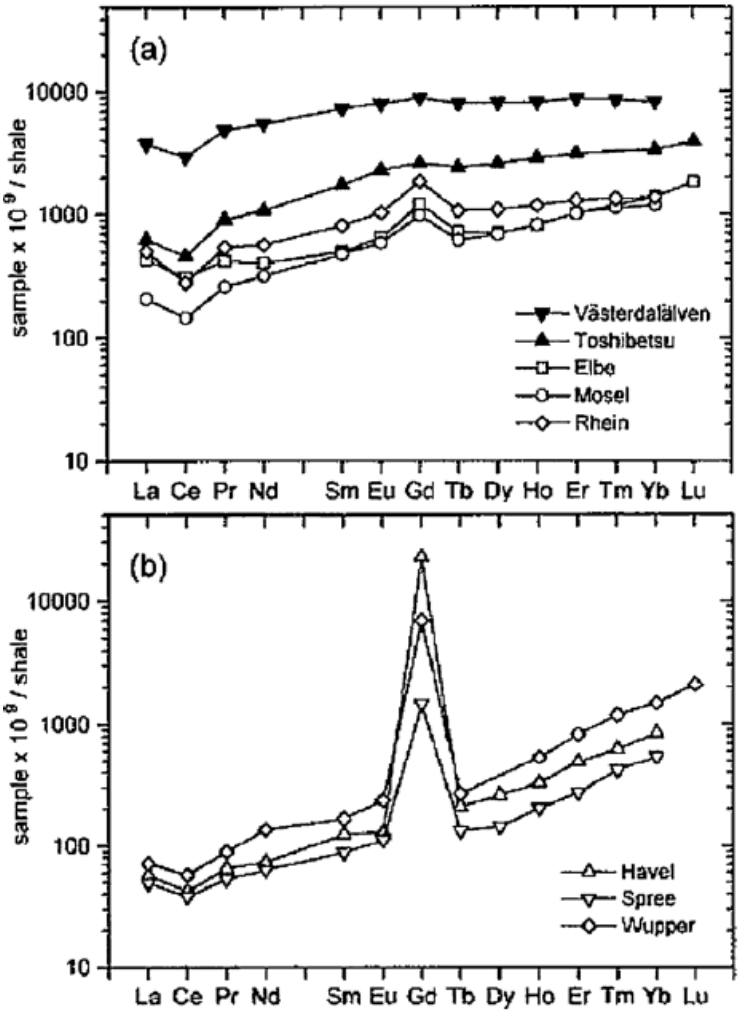

Figure 12. Normalized REE patterns of rivers draining non-industrialized and thinly populated areas (Vasterdalalven-Sweden, Toshibetsu-Japan) and rivers draining heavily populated areas in Germany [58].

The examination of WWTP effluent showed an anomaly ratio (that compares anthropogenic Gd content to the geogenic background) of 1680. This significant output of Gd indicates the obvious anthropogenic nature of this REE. The ability of Gd to pass WWTF unaffected indicates the involvement of very stable and highly water soluble compounds. The source of the Gd anomalies was soon discovered to be Gd-based contrast agents, which were at that time applied during MRI examinations for several years. This important study was the starting point for many following examinations [59-72] and for the discussion about the impact of the agents on the environment [56].

2.2.4 Methods of determination

Various methods for the determination of Gd in waters but also body fluids and tissue have been described in recent years (Table 2.). The vast majority of utilized techniques for the detection of Gd-based contrast agents are mass spectrometry (MS) and optical emission spectrometry (OES), both using inductively coupled plasma (ICP) as ionization and excitation method. However, techniques employing ICP without previous separation can only reveal the total gadolinium content present in the sample, regardless the origin of the rare earth element (REE). Rare earth elements consist of Scandium, Yttrium and Lanthanides. They are all obtained in the earth, but mostly in the trace amounts. If the natural uncontaminated water is scanned for the presence of REE, the natural background (pattern) is obtained. For contaminated waters, the anthropogenic gadolinium concentration is approximated based on the other REE content, which are not used by humans and thus, can't contribute to the natural background pattern (subtraction of expected natural background). Other studies presented detection of Gd species also by methods such as: UV-Vis detection [76,77,81,87,97], radioactivity detection [113], SEM [82] (scanning electron microscope), etc. Speciation analysis was achieved mostly by incorporating the hydrophilic interaction chromatography [64,90,105,109,110] (HILIC), and some of CA's were also successfully separated by classical reverse phase liquid chromatography. Because of the wide range of contrast agents used, and due to their different characteristics, the methods are various. The overview of methods used in recent years (including the experimental details) is summarized in Table 2.

Table 2. Overview of detection techniques for Gd-based contrast agents in different aqueous media. MP, mobile phase; BGE, background electrolyte; em., emission wavelength; ex., excitation wavelength; Rad., radioactivity detection; WE, working electrode; RE, reference electrode. Analytes: 1, Total Gd; 2, Gd(III) ion; 3, Gd-DTPA; 4, Gd-BOPTA; 5, Gd-DTPA-BMA; 6, Gd-DTPA-BMEA; 7, Gd-DOTA; 8, Gd-BT-DO3A; 9, Gd-HP-DO3A; 10, DTPA; 11, Gd-EDTA; 12, Gd-DTPA-BP; 13, Gd-DTPA-MMA; 14, Gd-DO3A; 15, Gd-NP-DO3A; 16, Gd-EOB-DO3A; 17, Cu-DTPA; 18, Fe-DTPA; 19, Zn-DTPA; 20, REE.

Author	Year	Ref.	Analytes	Analytical methods	Experimental details	LOD
Abraham	2007	82	1	SEM	SEM: acc. 20 keV, 15-16 mm distance	n/a
Abraham	2008	75	1	SIMS	SIMS: $^{157}Gd^{+}$, $^{158}Gd^{+}$, and $^{160}Gd^{+}$ Beam: 5.5 keV, 100 nA	n/a
Andrasi	2011	76	3,4,5,7,6	MEKC/UV-Vis	CE: 25 kV, BGE:SDS, phospate UV: 200 nm	0.4-20 μM
Arburgi	1998	77	4	HPLC/UV-Vis	HPLC: C8, 0.18% n-octylamine UV: 200nm	0.24 nM(plasma), 0.47 nM (urine), 2.6 nM (feces), 0.63 nM (bile), 2.8 nM (liver)
Bau	1996	58	1,20	ICP-MS	n/a	n/a
Bau	2006	60	1,20	ICP-MS	n/a	0.01-0.1 pg m/L
Behra-Miellet	1998	78	3,5,7	ESI-MS HPLC/ESI-MS	HPLC: C18, MP: 0.1% TFA water/AcN (gradient) Quadrupole ESI-MS: pos. ionization	n/a
Cacheris	1990	79	5, 12	Pot. Titration UV Computation	AgCl reference combination electrode UV: 268 nm	n/a
Campa	2005	80	4	CE/UV-Vis CE/ESI-MS	CE: 20kV, BGE: 50 mM NH_4HCO_3, pH 8.0; UV: 195 nm and 210 nm Ion-trap MS (positive and negative ionization)	1μM
Chellquist	1993	81	3	HPLC/UV-Vis	HPLC: PRP-X100, MP: 0,1 mM TRIS, 0.025 mM KCl, 1 mM EDTA, pH 8.0 UV: 272 nm	n/a

Table 2. (Continued) Overview of detection techniques for Gd-based contrast agents in different aqueous media. MP, mobile phase; BGE, background electrolyte; em., emission wavelength; ex., excitation wavelength; Rad., radioactivity detection; WE, working electrode; RE, reference electrode. Analytes: 1, Total Gd; 2, Gd(III) ion; 3, Gd-DTPA; 4, Gd-BOPTA; 5, Gd-DTPA-BMA; 6, Gd-DTPA-BMEA; 7, Gd-DOTA; 8, Gd-BT-DO3A; 9, Gd-HP-DO3A; 10, DTPA; 11, Gd-EDTA; 12, Gd-DTPA-BP; 13, Gd-DTPA-MMA; 14, Gd-DO3A; 15, Gd-NP-DO3A; 16, Gd-EOB-DO3A; 17, Cu-DTPA; 18, Fe-DTPA; 19, Zn-DTPA; 20, REE.

Author	Year	Ref.	Analytes	Analytical methods	Experimental details	LOD
Chellquist	1993	81	3	HPLC/UV-Vis	HPLC: PRP-X100, MP: 0.1 mM TRIS, 0.025 mM KCl, 1 mM EDTA, pH 8.00 UV: 272 nm	n/a
Elbaz-Poulichet	2002	83	1,2	ICP-MS	n/a	0.5 pM (Lu) 0.8 pM (Nd)
Frenzel	2008	84	2,3,4,5,6,7,8,9,16	HPLC/ICP-MS	HPLC: chealting Sepharose^{TM}, MP: 10 mmol/L bis-tris-buffer, pH 6, ICP-MS: ^{158}Gd	n/a
Hagan	1988	85	1,2,3,7,11	HPLC/fluorescence ICP-OES	HPLC: C18, MP: 50 mM tris base, 2 mM EDTA, pH 7.3 Fluorescence: ex. 280 nm, em. 316 nm, ICP-OES: n/a	n/a
Haustein	1990	86	1	ICP-OES	ICP-OES: 342.247 nm	60 nM (blood)
Hvattum	1995	87	3,5,13	HPLC/UV-Vis	HPLC: C18, 10 mM TEAA, 2 mM EDTA, pH 6.5- 7.0; Post-collumn reagent: 0.15 mM Arzenazo III; 0,1 M HNO_3, 0.01 M urea UV: 658 nm	0,3 μM
Joffe	1998	88	1	ICP-OES	n/a	n/a
Kahakachi	2009	89	3,4,5,6,7,9	HPLC/ICP-OES	HPLC: C18, MP: 10 mM NH_4AC ICP-OES: 242.246 nm	50 nM

Table 2. (Continued) Overview of detection techniques for Gd-based contrast agents in different aqueous media. MP, mobile phase; BGE, background electrolyte; em., emission wavelength; ex., excitation wavelength; Rad., radioactivity detection; WE, working electrode; RE, reference electrode. Analytes: 1, Total Gd; 2, Gd(III) ion; 3, Gd-DTPA; 4, Gd-BOPTA; 5, Gd-DTPA-BMA; 6, Gd-DTPA-BMEA; 7, Gd-DOTA; 8, Gd-BT-DO3A; 9, Gd-HP-DO3A; 10, DTPA; 11, Gd-EDTA; 12, Gd-DTPA-BP; 13, Gd-DTPA-MMA; 14, Gd-DO3A; 15, Gd-NP-DO3A; 16, Gd-EOB-DO3A; 17, Cu-DTPA; 18, Fe-DTPA; 19, Zn-DTPA; 20, REE.

Author	Year	Ref.	Analytes	Analytical methods	Experimental details	LOD
Knappe	2005	57	1,2	ICP-MS	n/a	0.01 – 0.1 pg/mL
Kindberg	2010	91	1,5	Rad. Detection ICP-OES ICP-SF-MS	Rad.: Gd[^{14}C]DTPA-BMA ICP-OES: 336.223 and 342.247 nm ICP-MS: ^{157}Gd	0.1 μg Gd/g Tissue (ICP-OES)
Kulaksiz	2007	69	1,2	ICP-MS	n/a	n/a
Kümmerer	2000	63	1	ICP-MS	ICP-MS: ^{156}Gd, ^{157}Gd, ^{158}Gd, and ^{160}Gd ICP-MS: ^{158} Gd	1 μg/L
Künnemeyer	2008	90	1,3,4,5,7,8	HPLC/ESI-MS ICP-OES	HPLC: zic-HILIC, MP: 76% 12.5 mM NH4FA, 24% AcN, (pH 3.75) Ion-trap MS (possitive ionization) ICP-OES: 335.047, 336.223, and 342.247	0.1 - 10 μM
Künnemeyer	2009	92	1,3,4,7	CE/ESI-MS ICP-OES	CE: 30 kV, BGE: 25 mM morpholine, 12.5 mM AcOH, pH 8.0 ESI-ToF-MS: positive ionization ICP-OES: 335.047, 336.223, and 342.247 nM	0.2 μM
Künnemeyer	2009	93	3,10,17,18,20	CE/ESI-MS ICP-OES	CE: 30 kV, BGE: 25 mM morpholine, 12.5 mM AcOH, pH 8.0 ESI-ToF-MS: positive ionization ICP-OES: 335.047, 336.223, and 342.247 nM	(CE): 500 nM (3), 1 μM (10,18)
Künnemeyer	2009	64	1,3,4,5,7,8	HPLC/ICP-MS	HPLC: zic-HILIC, MP: 76% 12.5 mM NH4FA, 24% AcN (pH 3.75)	1 nM

Table 2. (Continued) Overview of detection techniques for Gd-based contrast agents in different aqueous media. MP, mobile phase; BGE, background electrolyte; em., emission wavelength; ex., excitation wavelength; Rad., radioactivity detection; WE, working electrode; RE, reference electrode. Analytes: 1, Total Gd; 2, Gd(III) ion; 3, Gd-DTPA; 4, Gd-BOPTA; 5, Gd-DTPA-BMA; 6, Gd-DTPA-BMEA; 7, Gd-DOTA; 8, Gd-BT-DO3A; 9, Gd-HP-DO3A; 10, DTPA; 11, Gd-EDTA; 12, Gd-DTPA-BP; 13, Gd-DTPA-MMA; 14, Gd-DO3A; 15, Gd-NP-DO3A; 16, Gd-EOB-DO3A; 17, Cu-DTPA; 18, Fe-DTPA; 19, Zn-DTPA; 20, REE.

Author	Year	Ref.	Analytes	Analytical methods	Experimental details	LOD
Lawrence	2010	94	1,2	ICP-MS	n/a	n/a
Loreti	2004	96	2,3	SEC/ICP-MS	HPLC: BioSep-SEC-S3000, MP: 20 mM Tris-HCL, pH 7.4 ICP-MS: ^{155}Gd, ^{156}Gd, ^{157}Gd, ^{158}Gd, and ^{160}Gd	n/a
Larusso	1994	97	4	HPLC/UV-Vis	HPLC: C8, MP: 74% 6.8 mM $TBAH_2PO_4$, 26% AcN	1.1 μM (plasma) 7.6 μM (urine), 1.7 μM (bile)
Mazzucotelli	1995	98		HPLC/ICP-OES	HPLC: C8, MP: 0.01 mol/L KH_2PO_4, 12% (v/v) MeOH ICP-OES: 342.238 nm, ultrasonic nebulizer	15.9 μM
Möller	2002	99	1,2	ICP-MS	n/a	n/a
Morteani	2006	95	1,2	ICP-MS	n/a	n/a
Moutiez	1997	100	2,3,7	HPLC/TRL	Lum.: ex. 274 nm, em. 313nm HPLC: C8, MP: TRIS-HCL, 7.8% AcN, pH 7.6	n/a
Normann	1995	101	5	HPLC Rad. Detection	HPLC: beta-cyclodextrin column Rad.: ^{154}Gd	n/a
Nozaki	2000	102	1,2	ICP-MS	n/a	n/a
Okada	2001	103	1	ICP-OES	n/a	n/a
Puttagunta	1996	104	1	ICP-OES	n/a	n/a
Rabiet	2009	65	1,2	ICP-MS	n/a	n/a

Table 2. (Continued) Overview of detection techniques for Gd-based contrast agents in different aqueous media. MP, mobile phase; BGE, background electrolyte; em., emission wavelength; ex., excitation wavelength; Rad., radioactivity detection; WE, working electrode; RE, reference electrode. Analytes: 1, Total Gd; 2, Gd(III) ion; 3, Gd-DTPA; 4, Gd-BOPTA; 5, Gd-DTPA-BMA; 6, Gd-DTPA-BMEA; 7, Gd-DOTA; 8, Gd-BT-DO3A; 9, Gd-HP-DO3A; 10, DTPA; 11, Gd-EDTA; 12, Gd-DTPA-BP; 13, Gd-DTPA-MMA; 14, Gd-DO3A; 15, Gd-NP-DO3A; 16, Gd-EOB-DO3A; 17, Cu-DTPA; 18, Fe-DTPA; 19, Zn-DTPA; 20, REE.

Author	Year	Ref.	Analytes	Analytical methods	Experimental details	LOD
Raju	2010	105	1,3,4,5,7,8	HPLC/ICP-MS ICP-MS	HPLC: zic-HILIC, MP: 60% 20 mM NH_4Ac, 40% AcN (pH 3.75) ICP-MS: ^{158}Gd	22 ng/L
Sausserau	2008	106	1	ICP-MS	^{157}Gd	n/a
Schumann	1991	107	1	ICP-OES	ICP-OES: 342.247 nm	n/a
Telgmann	2011	108	1	TXRF	TXRF: Ex.: 50 kV, 750 mA, t = 1000s	100 µg/L (urine) 80 µg/L (plasma)
Telgmann	2012	109	3,7,18	HPLC/ESI-MS EC/LC/ESI-MS EC/LC/ICP-MS	HPLC: HILIC/PGC Orbitrap MS (positive ionozation) CE: 30 kV, BGE: 25 mM morpholine, pH 8.0 LC: PGC, MP: 25 mM NH_4Ac, pH 5.0	50 nM (Fe-DTPA)
Telgmann	2012	110	1,2,3,4,5,7,8, 11,20	ICP-MS HPLC/ICP-SF-MS IC/ICP-MS	Isotope dilution: ^{158}Gd enriched Gd_2O_3, ^{156}Gd, ^{158}Gd,and ^{160}Gd; mass bias correction: $^{203}Tl/^{205}Tl$ HPLC: solid core HILIC, 30% 50 mM NH_4Ac (pH 3.75), 70% AcN IC: cation exchange, Nucleosil 5 SA 125/4.0	HPLC/ICP-SF-MS 0.82 nM

Table 2. (Continued) Overview of detection techniques for Gd-based contrast agents in different aqueous media. MP, mobile phase; BGE, background electrolyte; em., emission wavelength; ex., excitation wavelength; Rad., radioactivity detection; WE, working electrode; RE, reference electrode. Analytes: 1, Total Gd; 2, Gd(III) ion; 3, Gd-DTPA; 4, Gd-BOPTA; 5, Gd-DTPA-BMA; 6, Gd-DTPA-BMEA; 7, Gd-DOTA; 8, Gd-BT-DO3A; 9, Gd-HP-DO3A; 10, DTPA; 11, Gd-EDTA; 12, Gd-DTPA-BP; 13, Gd-DTPA-MMA; 14, Gd-DO3A; 15, Gd-NP-DO3A; 16, Gd-EOB-DO3A; 17, Cu-DTPA; 18, Fe-DTPA; 19, Zn-DTPA; 20, REE.

Author	Year	Ref.	Analytes	Analytical methods	Experimental details	LOD
Telgmann	2012	74	3,4,5,7,8	EC/ESI-MS EC/CE/ESI-MS EC/CE/ICP-MS EC/LC/ESI-MS EC/LC/ICP-MS	EC: WE: BDD, RE: Pd/H_2, 0-2500 mV ESI-MS: ToF (positive) or Orbitrap (positive) ICP-MS: ^{158}Gd, CE: 30kV, BGE: 25 mM morpholine, pH 8.00 LC: PGC, MP: 25 mM NH_4Ac, pH 5.00	n/a
Tweedle	1991	111	3,7,9	HPLC/UV-Vis	HPLC: C18, 50 mM, MP: TrisAc, 2 mM	n/a
Verplanck	2010	112	1,2	ICP-MS	n/a	n/a
Vora	1986	113	2,3,10	HPLC/UV-Vis Rad. Detection	HPLC: C18; MP: 90% 5 mM KH_2PO_4, 10% AcN, pH 7.00 UV: 200 nm; Rad.: ^{153}Gd	n/a
Weinmann	1984	114	3	HPLC/UV-Vis ICP-OES	HPLC: C8, 17% MeOH, 83% TBA perchlorate UV: 238 nm ICP/OES: n/a	1 umol/L (ICP-OES)
Zhu	2004	115	1,2	ICP-MS	n/a	0.003-0.027 ng

2.3 Thermal lens methods

2.3.1 Thermal lens effect

Thermal lens effect occurs in high power laser beams propagating in an absorbing medium. When a high power laser beam propagates through an absorbing medium, a small portion of its energy is absorbed by the medium. For a Gaussian laser beam propagating through a sample of absorbing material, more energy is absorbed at the axis of the beam where light intensity is the highest. This absorption of light energy results in local heating of the medium because of radiationless deexcitation processes through which the absorbed energy is released. Heating leads to change in the local temperature of the medium. Since refractive index of the medium is temperature dependent, absorption of laser light ultimately results in creation of a non-uniform refractive index of the medium along the propagation of laser beam. Such non uniform refractive index (refractive index gradient) depends on the power density of the laser beam and on the thermal properties (temperature coefficient of the refractive index, thermal conductivity) of the medium along the beam path. The refractive index gradient can be considered as a lens like element, which increases the beam divergence [116]. The thermal lens effect is observable for laser beams in the power range of only microwatts in samples normally thought to be transparent, and thus it is suitable for the low absorption measurements of nonfluorescent samples. Its sensitivity is higher than that of the conventional transmission or reflectance techniques because, in this technique the signal is directly proportional to the absorbed energy and therefore to the excitation power [117].

The thermal lens signal can be expressed as:

$$S(z,t) = \frac{\pi P_e \alpha \eta l}{2\lambda_p k} \frac{\mathrm{d}n}{\mathrm{d}t} \qquad (2.16)$$

Where: *S*- signal, *z*- sample position, *t*- time, P_e- total excitation light power, α- absorption coefficient, *l*- sample's length, *k*- thermal conductivity, d*n*/d*t*- temperature coefficient of the refractive index, λ_p- probe beam wavelength, η- intracavity amplification factor.

2.3.2 Instrumentation

Based on the principle of the instruments operation, TLS instuments can be classified into two groups: (i) single-beam, and (ii) dual-beam or pump-probe instruments. Besides this classification, dual beam instruments can be divided according to the optics used into:

classical thermal lens spectrometers (TLS) and thermal lens microscopes (TLM). Thermal lens microscopes are primarily developed for the microfluidic systems, because they possess an extra microscope-like lens, which grants better focusation of the beams.

2.3.2.1 Single-beam instruments

Single-beam instruments are using the same laser beam to excite the sample and in the same time to probe the thermal lens generated. This kind of instruments, were initially developed to study the dependence of thermal lens effect on parameters such as laser power, beam divergence, sample length, concentration, convection, and flow. Single-beam instruments are relatively simple to build, and easy to operate when compared to dual-beam instruments.

The laser beam is focused with a lens and modulated at low frequency (or just On-Off). After passing through the sample, the beam center intensity is usually measured in the far field with a photodiode placed behind a pinhole. The photodiode output is amplified and fed into a storage oscilloscope which facilitates the recording of transient changes in the beam intensity [118].

The choice of suitable laser is critical, and usually the first step in the construction of instrument. To obtain required sensitivity, the laser must possess the sufficient power and also the correct wavelength, based on the compound which we want to detect, and its absorption spectrum. Various lasers are available and among these, Ar lasers are widely used due to their versatility and possibility of intracavity frequency doubling in cw mode (several discrete wavelengths in the 244 – 514.5 nm range). Except Ar lasers, also other types can be used such as: He-Cd lasers (441.6nm), He-Ne lasers (632.8 nm), Kr lasers (from 476.2 to 799.3 nm), semiconductor and continuously tunable dye lasers [118].

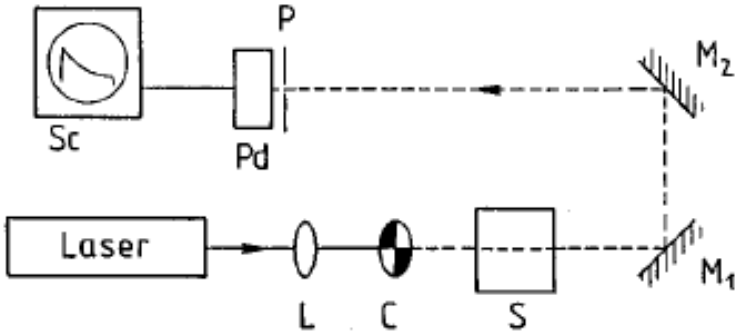

Figure 13. Schematic diagram of a single-beam instrument: L,lens; C, chopper; S, sample cell; M1, M2, mirrors; P, pinhole; Pd, photodiode; Sc, scope [118].

2.3.2.2 Dual-beam instruments

In a dual-beam instruments is the generation and detection of the thermal lens is achieved separately by a modulated pump beam and a nonmodulated probe beam respectively. A high power laser usually serves as a source of the pump beam, while the probe beam is usually relatively weaker. To focus the excitation (pump) beam directly on the sample and to mismatch the beam waist of the pump and probe beams, separate lenses are used. This allows the highest thermal lens strength. Significant spatial overlapping of both beams inside the sample is essential for good sensitivity. The generated thermal lens produces fluctuations in the intensity of the probe beam that can be sensitively monitored by signal averaging devices e.g. lock-in amplifiers.

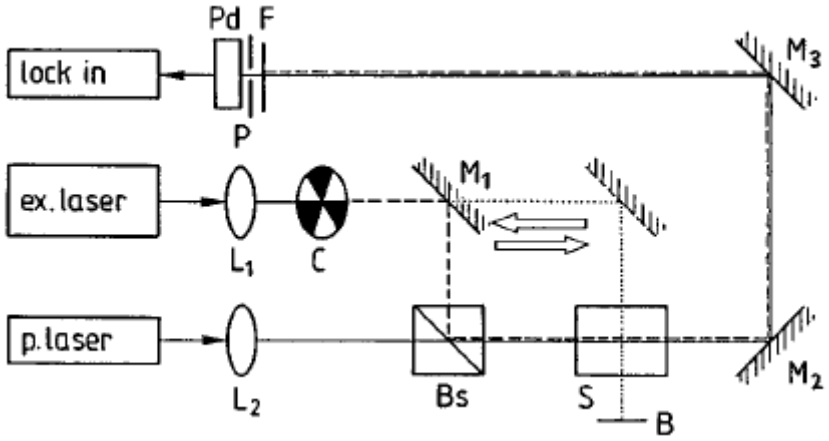

Figure 14. Schematic diagram of a dual beam thermal lens instrument with a possibility of collinear (- - -) or transverse (...) propagation of the pump beam relative to the probe beam(- - -): ex, excitation laser; p, probe laser; L_1 and L_2, lenses; C, chopper; Bs, beamsplitter; S, sample cell; B, beam blocker; M1 – M3, mirrors; F, filter; P, pinhole; Pd, photodiode[118].

On the Fig.14 are two possible configurations of the pump beam direction: transversal or collinear. Transversal configuration is particularly useful for samples which are available in small volume, and for chromatographic detection. The collinear configuration, on the other hand provides better absolute sensitivity because of the longer interaction length of the two beams.

The choice of pump laser is wider here because pulse lasers are also suitable for excitation purposes. Possible types are: He-Ne, He-Cd, Ar, Kr, dye and semiconductor, pulsed dye lasers for visible light, nitrogen, frequency doubled and frequency mixed Nd^{3+}: YAG lasers for UV light; fundamental Nd^{3+}: YAG and Ti-sapphire lasers for the near IR. Again the choice depends on the compound which we want to detect, and the sensitivity is depending on the power.

For the probe beam, lasers with high stability should be chosen. The power of the probe beam is not important here unlike for pump laser. Therefore, He-Ne lasers are usually used, because they are well known for their stability and reliability [118].

2.3.3 TLS applications

Thermal lens spectrometry is highly sensitive spectroscopic technique for measurements of liquid samples, where it enables determinations of optical absorbances lower than 10^{-6} [119]. It is not so common method in the routine analysis because of the limited availability of suitable laser sources, especially UV wavelengths. The major disadvantage is the poor selectivity, and limited tuneability. This is because TLS instruments are unable of simultaneous multiwavelength detection. TLS has a fast response and is therefore a suitable detection method for liquid flows e.g.: high performance liquid chromatography (HPLC), capillary electrophoresis (CE), ion chromatography (IC) or flow injection analysis (FIA). Separation techniques can discriminate several analytes, while TLS provides high sensitivity as well as the possibility of probing small amounts of samples. High specificity can also be achieved with TLS methods by applying the concepts of biorecognition exploiting various biomolecules such as enzymes and antibodies [121].

2.3.3.1 TLS detection in high performance liquid chromatography

Spectrophotometric detectors in HPLC are the most spread and versatile detectors. Sensitivity of this detector is determined by the optical path length in the cell. On going to capillary and microcolumn chromatographic systems, the sensitivity is strongly decreased when the capillary size becomes as large as several micrometers.

TLS is successfully used in HPLC for the detection of organic and also inorganic compounds [122-125]. The application of thermal lens detectors, lowers the limits of detection (LOD) by two or three orders of magnitude, when compared to spectrophotometric detectors [122,126]. The majority of publications are describing application of TLS detection coupled with HPLC for determination of organic compounds like for example: carotenoids [124,127], catecholamines [128], or amino acids [129].

2.3.3.2 TLS detection in flow injection analysis

TLS has a great importance in FIA [123,125,130,131], as the universal detector for this technique is currently not available, and the choice of detector is mostly depending on the analytical application of the system [121,133-135]. When peristaltic pumps are used the main problem of detection in FIA is the noise caused by flow fluctuation, particularly in case of TLM detection [136]. This problem was resolved by using pulseless syringe pumps.

2.3.3.3 TLS detection in capillary electrophoresis

Spectrophotometric detection, is currently the most reliable and universal technique for detection in capillary electrophoresis (used in about 4/5 of all works). Photothermal methods, which combine the advantages of spectrophotometric and refractometric detection techniques and possess high sensitivity, are however considered as one of the best detection techniques in capillary electrophoresis. Due to this fact, TLS is currently actively developed in this area [121,137-142].

2.3.3.4 TLS detection in microfluidic systems

Applications of TLS in flow injection analysis (FIA) and TLM in combination with FIA on microchemical chips was recently reported [120, 121]]. Microchip implementation provides high sample throughput, reduced operational costs, simplicity and high reproducibility. This is well suited for rapid screening of various samples for presence of non-desired compounds e.g. pesticides, allergens and others. Coupling with FIA technique also provides an elegant solution, how to avoid losses of sensitivity or systematic errors due to degradation of analytes, uder high intensity light from lasers [121]. TLM makes it possible to characterize reactions in small volumes (to 1 μm^3) with reagent concentrations at a level of nanograms and also to count single molecules [143-148]. TLM is also used as a detection technique in various separation methods [132,146,149-150].

3. THE SUBJECT OF STUDY

Subject of degradation study is at this moment probably the most widespread Gd-based contrast agent Gadobutrol (Gd-BT-DO3A). Even though the Gd anomaly is in recent years actively monitored, little is known about the contrast agents chemical behavior in environment or in the waste water treatment plant processes regarding degradation and the formation of transformation processes. Nevertheless, there were some studies recently about stability of these compounds towards UV radiation [152], and also ozone [153]. It was revealed that Gadobutrol is extremely stable chelate, resistant to UV radiation. For some reason, no one tried to degrade this compound by TiO_2 assisted photocatalysis. The degradation of this compound can be however questionable, because in its stable chelated form, gadolinium shows no toxicity, but it is well known that the free Gd^{3+} ions are toxic for the environment, and in human body when released from contrast agent, they may induce the nephrogenic fibrosing dermopathy (NFD) and nephrogenic system fibrosis (NSF). Critical group of people which are likely to suffer from this disease, are the patients with decreased renal function. NSF is a distressing and debilitating condition that causes exhibition of fibrosis on the skin, joints, eyes and internal organs, hardened skin, fibrotic nodules and plaques [154-156]. No effective therapy is currently available, although successful renal transplantation or resolution of underlying acute kidney injury may stabilize the fibrosing process and in some cases reverse some of the clinical symptoms [157].

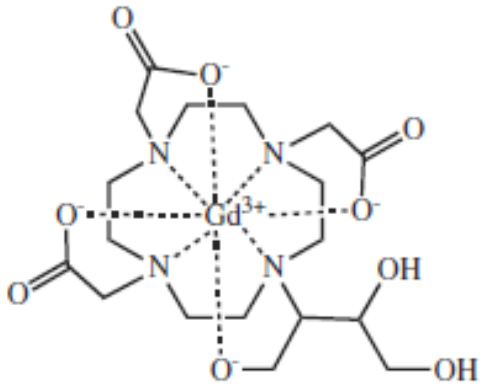

Gd-BT-DO3A
(Gadovist®)

Figure 15. Chemical structure of the subject of our interest, with commercial name included.

This chelate compound, was designed to resist the metabolic processes in human body. It is highly hydrophilic and belongs to the macrocyclic, non-ionic Gd-based contrast agent family. The molecule consists of neutral Gd(III) central atom, coordinated by four nitrogens, three monodentate carboxyle oxygens, and one hydroxyalkyl oxygen. High stability is achieved by trapping the Gd(III) atom in the middle of 1,4,7,10-Tetraazocyclododecane [158].

Table 3. Some of the main characteristics of studied compound [159].

Name	Gadobutrol
CAS	138071-82-6
Molecular weight	604.712 g/mol
Osmolarity	1117 mOsm/Kg (37°C)
Viscosity	4.96 mPa (37°C)
log P(n-octanol/water)	-5.4 (25°C)

4. THE AIM OF THE WORK

The aim of this study was to develop or optimize existing method which could be used for degradation experiment monitoring, by thermal lens effect-based detection techniques. The substance which was chosen for degradation experiments is nowadays widely used contrast agent for magnetic resonance imaging which can be found in the wastewater treatment plants effluents [63]. This indicates that, the conventional water treatment processes are not sufficiently effective in terms of contrast agents removal. Only a little is known about degradation of gadolinium-based MRI contrast agents and so far, there are no published studies about photocatalytic degradation of these compounds.

5. EXPERIMENTAL PART

5.1 Instrumentation

- Furnance, EUP-K 6/1200 Laboratory furnace, Bosio d.o.o. Slovenia
- Elcometer 501 pencil hardness tester, Elcometer
- Stemi^{TM} DV4 Stereomicroscope, Carl Zeiss
- Arctic A25 refrigerated circulator, Thermo Scientific
- Ozonator, LAB series, Pacific Ozone
- Prototype photoreactor
- TOC/TN analyzer, AG MULTI N/C 3100, Analytik Jena
- Tempered water bath, JB Aqua 5 Plus, Grant
- Spectrophotometer, HP 8453E, Hewlett-Packard GmbH
- TLM spectrometer, pump beam source: 532 nm solid-state laser, 10 mW, Flex, B&VTEC inc. ; probe beam source: 660 nm-solid state laser, 100 mW, CUBE 600-100C, Coherent inc.
- pH meter, HI 8417 ; HI 1131 – glass electrode; Hanna Instruments

5.2 Software

- Microsoft office 2007
- OriginPro 8.5
- Adobe Illustrator CC 2015
- MATLAB 7.4.0 (R2007a)
- multiWin, TOC software

5.3 Chemicals

5.3.1 Photocatalyst preparation

- Highly pure water, NANOpure system, Barnstead
- Absolute ethanol, Sigma-Aldrich
- Hydrochloric acid; (37%), Sigma-Aldrich
- Lewasil 200/30%, colloidal SiO_2, H.C.Starck

- Titanium dioxide nanopowder, Aeroxide® P25 (80% Anatase, 20% Rutile), Evonik Degussa
- 1F solution, mixture of $HClO_4$, TTIP, EtOH, H_2O (see [151] for details)
- 396W solution, mixture of TEOS, HCl and H_2O (see [151] for details)

5.3.2 Degradation experiments and analysis

- Methylene blue hydrate; 96%, Fluka Analytical
- Gadobutrol, Gadovist (7.5 mL injection, 1 mM/mL), Bayer HealthCare Pharmaceuticals inc.
- Gadolinium (III) nitrate hydrate; 99.9% (REO), Alfa Aesar
- 1-(2-Pyridylazo)-2-naphtol (PAN); 98%, Alfa Aesar
- Hexadecyltrimethylammonium bromide (CTAB), ≥99%, Sigma-Aldrich
- Ammonium chloride, extra pure, Riedel-de Haën AG.
- Ammonium hydroxide; 25%, J.T.Baker

5.3.3 Toxicity assessment

- Calcium chloride, Sigma-Aldrich
- Magnesium sulfate, Fluka Analytical
- Sodium bicarbonate, Sigma-Aldrich
- Potassium chloride, Sigma-Aldrich

5.4 Catalyst preparation

5.4.1 Titania/binder sol preparation

Catalyst was prepared according to the SI 23585 A (Šuligoj, A.) patented preparation procedure of durable titania coatings [151] as follows:

Given volumes (Tab.4) of 1F (nanocrystalline titania sol), 396W (silica sol), Levasil 200/30% (colloidal SiO_2) and absolute ethanol were mixed together in the beaker to create a binder sol. While rapid mixing with magnetic stirrer, P25 powder was slowly added. The suspension was than mixed for 1 hour and after stored in fridge for further use.

Table 4. Amounts of reagents used for catalyst preparation.

1F [151]	396W[151]	Levasil 200/30%	EtOH	TiO_2 P25
10.5 mL	1.5 mL	25 mL	10 mL	4 g

5.4.2 Slides preparation

Glass slides (1.2 cm x 28 cm x 0.1 cm) were cleaned by ethanol. Layers of photocatalyst were then applied on the glass surface by brush (it is important to do each side of the glass by just one slow movement). After application, slides were dried with hair dryer, placed in a holder, and finally treated in the furnace at 150°C for 1 hour. This cycle was repeated 3 times, to obtain sufficient catalyst surface density.

5.5 Catalyst characterization

5.5.1 Mechanical resistance of the layers

Mechanical resistance of prepared slides was tested by the Wolff-Wilborn pencil hardness test, fully described in BS 3900-E19, ISO 15184 and ASTM D 3363-92a. Each pencil from the set, starting with hardest 6H and ending with softest 2B was one by one attached to trailer-like pencil lead under the contact angle of 45°. Pencil lead was after placed on the glass slide with photocatalyst, and pulled for about 1cm along. After each pencil, the surface was checked by stereomicroscope with LED illumination, wheter there is a scratch or not. The hardness of TiO_2 layers was proved to resist 1H and softer.

5.5.2 Photocatalytic activity

For photocatalytic activity evaluation, methylene blue (MB) was chosen as a model compound. Experiment was carried out in a house-made reactor, described in chaper **5.6.1**. 60 mL of MB solution (4 μM) in deionized water was degraded in the reactor cell, firstly by prepared slide and secondly, by P25 Aeroxide® powder with concentration of 0.1 g/L. Degradation efficiency was than monitored spectrophotometrically by measuring the absorbance decrease at λ = 664 nm.

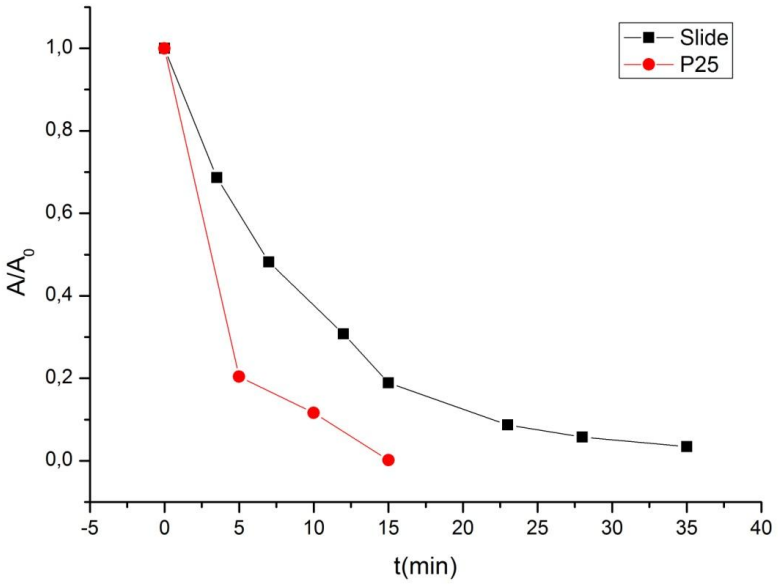

Figure 16. Absorbance decrease of MB for λ = 664 nm with time for both P25 (circle) and slide (square).

Fig.16. shows, that the time which was needed for complete removal of methylene blue from the solution, is more than twice higher for the slides. From the slope values of linearized plot equations (Fig.17), we can obtain rate constants *k.*

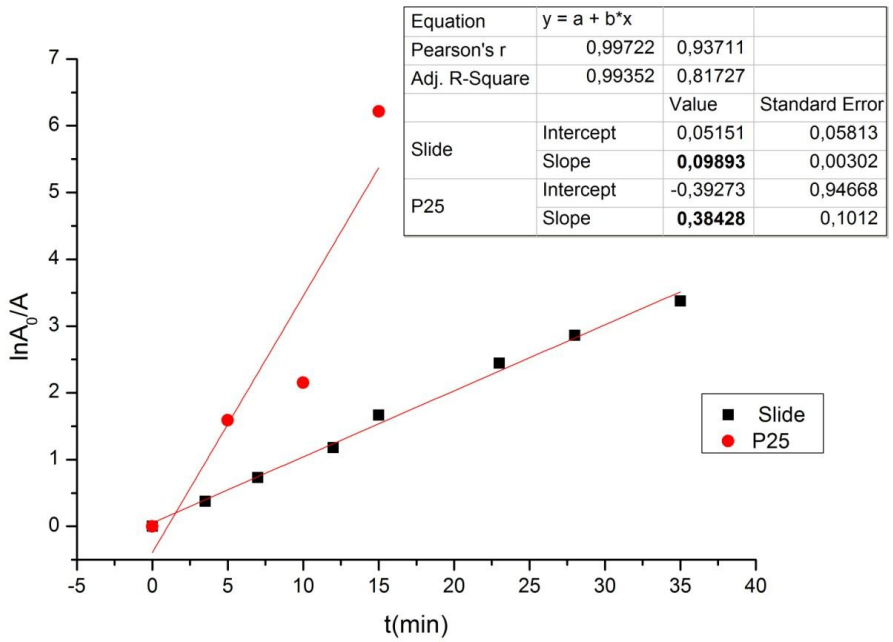

Figure 17. The kinetics of MB photocatalytic degradation, using P25 nanopowder (circle), immobilized TiO_2 (square).

Fig.17 reveals, that the kinetic rate constants *k*, are equal to 0.09893 min^{-1} and 0.39428 min^{-1} for the slide and P25 powder respectively.

However, the P25 powder works better, we decided to use by us prepared slides because of the practical reasons, when taking in account the real possibility of usage in wastewater treatment technologies. Usage of P25 powder in real WWTP processes is at the moment not feasible due to the problems with reusage of P25 powder and the separation from water in general.

5.6 Experimental set-up

5.6.1 Reactor

For our experiments, house-made prototype reactor was used. Reactor body is made of polished aluminium plate bended, especially to focus the light from the lamps to the middle of reactor where the reaction cell is attached. The reactor setup can be seen on Fig.18.

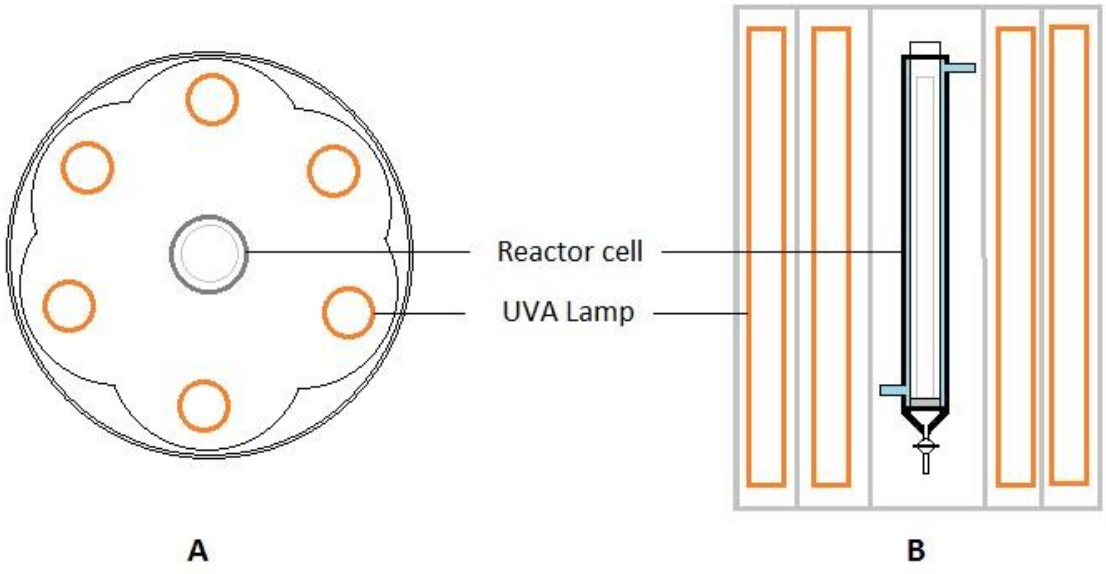

Figure 18. Prototype reactor: top view (A), side view (B)

5.6.2 Irradiation source

The reactor was equipped with 6 low-pressure mercury fluorescent lamps (CLEO, 43.8 cm x 2.6 cm, Philips) with 20 W power each. Emission maximum of these UVA lamps is at 355 nm.

5.6.3 Reactor cell

The reactor cell is made of DURAN® borosilicate glass. The body of reactor cell is coated with the water cooling system, which was used to maintain constant temperature of 24°C during all experiments. This was achieved with refrigerated bath circulator, which provided efficient cooling. During all experiments, the air (or ozone) was purged into the reactor through the glass frit with the valve. The volume of reactor cell is slightly more than 60 mL with dimensions of 40 cm in length, 1.85 cm and 22.7 cm inner and outer diameter respectively. Before each experiment, 1 slide with immobilized TiO_2 was inserted inside with tweezers.

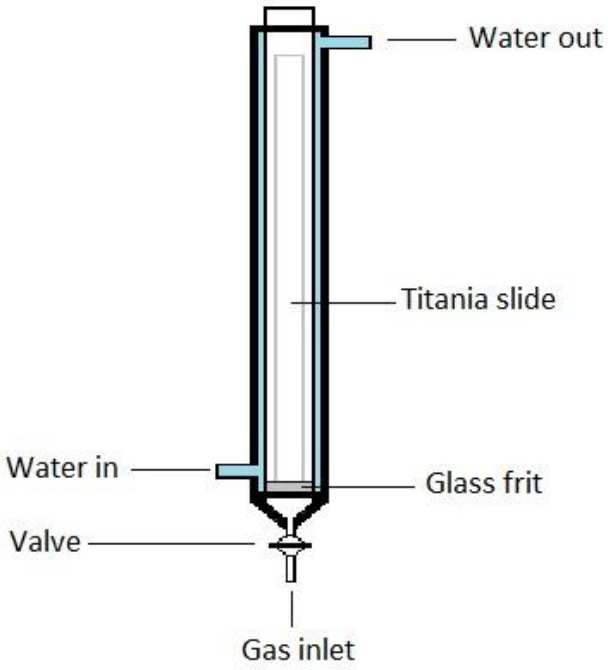

Figure 19. Scheme of the reactor cell.

5.7 Degradation experiments

All degradation experiments i.e. photocatalysis and ozonation, were carried out in the experimental set-up described above, performed in presence of P25 immobilized on the glass slide (TiO_2 + UV for photocatalysis), or without – ozone only (O_3 generator for ozonation).

Before each experiment, reactor cell was filled with 57mL of deionized water, and purged with synthetic air (79% N_2, 21% O_2), or ozone generated from oxygen feed gas by ozonator. After 15 minutes, 3 mL of 0.636 mM stock solution of gadobutrol in water was added and just before turning the lamps on (after another 15 min in the dark for photocatalysis), samples were taken for initial analysis. The amount of gadolinium in reactor remained for each experiment constant (5 mg/L). This solution was purged with air/ozone during the whole experiment duration. Due to the higher sample demand for further analysis, and relatively small volume of reactor cell, as well as preserving the contaminant/catalyst ratio, samples couldn't be taken in the process, but the whole volume of reactor cell was taken after the catalysis time (0 to 5 hours) was over. After degradation process, samples were stored in glass vials, wrapped in aluminium foil, at the tempereature of 4°C and consequently used for TOC (total organic carbon), UV-Vis or TLM (thermal lens microscope) analysis.

Ozonation was performed with the same contaminant concentration. Before introducing the pollutant into ozonated water, ozone concentration in solution after 15 minutes of purging was determined spectrophotometrically at 260 nm and directly calculated (Eq. 5.1). Its concentration was determined to be 6.5 mg/L.

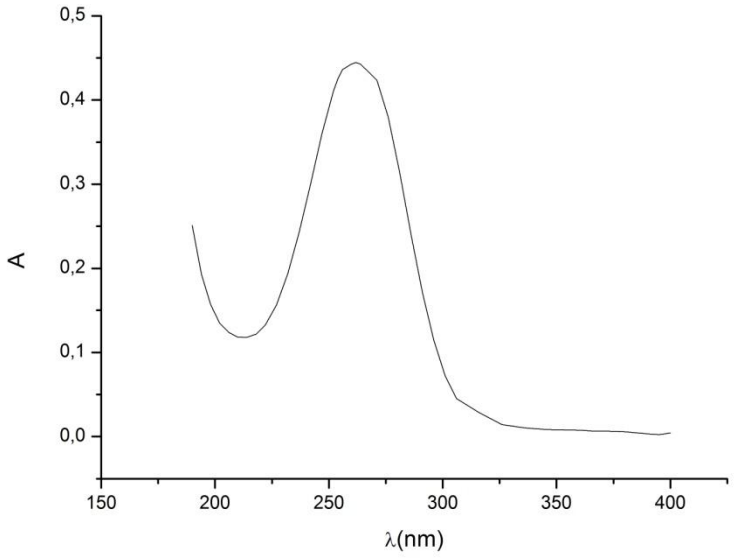

Figure 20. Absorption spectrum of Ozone in solution (c = 6.5 mg/L).

$$[O_3]\ (mg/L) = 14.59 \times A_{260} \qquad (5.1)$$

After the end of degradation experiments, samples were transferred into glass vials and left open over-night in the hood, and thus dissolved ozone could be naturally removed. Vials with solution were after stored under same conditions as previously described.

5.8 Methods of analysis

5.8.1 UV-Vis spectrophotometry

For spectrophotometric detection as well as for the thermal lens microscopy, method [160] based on the formation of metal complex was adapted and modified. For calibration, stock solution of Gd with concentration 38.16 μM (6 mg/L) was prepared by dissolving respective amount of gadolinium(III) nitrate hydrate (Alfa Aesar) in deionized ultrapure water.

Reagent solution, was prepared by dissolving 0.0187 g of 1-(2-Pyridylazo)-2-naphtol (PAN), and 0.4556 g of hexadecyltrimethylammonium bromide (CTAB), in ammonia buffer with pH= 9.22; in 500 mL volumetric flask. The whole mixture was than heated in water bath at 70°C for 5 hours to achieve better dissolution of PAN. Such prepared solution than had $c_{PAN} = 1.5\ x10^{-4}$ mol/L and $c_{CTAB} = 2.5\ x\ 10^{-4}$ mol/L. 500 mL of buffer was prepared by dissolving 8.0235 g of NH_4Cl with 19.425 mL of NH_4OH in water. 1600 μL of this final reagent solution was each time taken and mixed with 400 μL of sample solution/standard Gd solution.

Such prepared solutions were than measured after 25 minutes spectrophotometrically, using HP 8453 spectroscopy system, and subsequently with TLM system. Absorbance values at $\lambda = 532$ nm were recorded. All spectrophotometric measurements were conducted in 10 mm quartz cell.

Calibration measurements were conducted with respect to the blank, which consisted of given volume of reagent solution in surfactant (described above) and respective amount of deionized water.

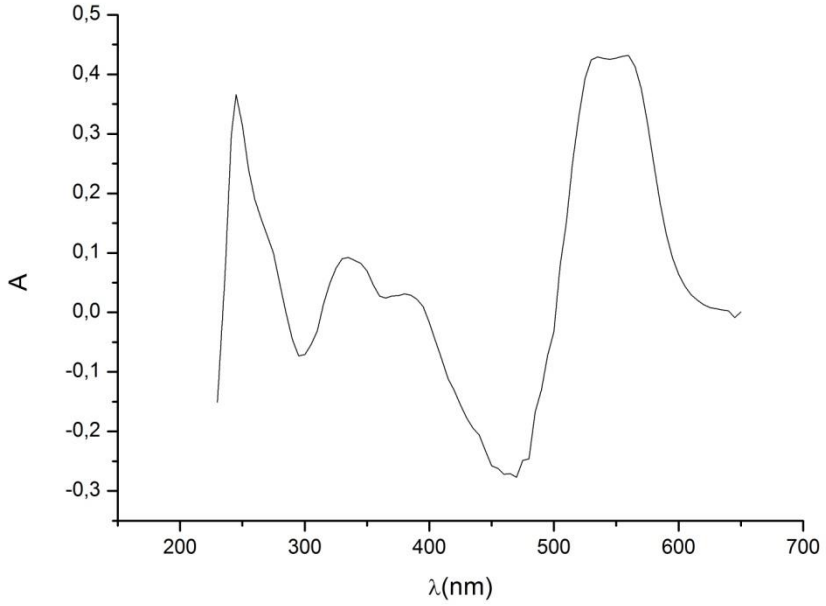

Figure 21. Absorption spectrum of Gd-PAN complex ($c_{Gd\text{-}PAN}$ = 7.632 μM in final solution); versus blank (c_{PAN} = 0.12 mM , c_{CTAB} = 0.2 mM)

5.8.2 Thermal lens microscope

For TLM measurements, double-beam instrument with collinear set-up was modified for our purposes. The original system consisted of 2 solid-state lasers, one of them 660 nm (red, which originally served as an excitation laser) with power of 100 mW, the second one 532 nm (originally as a probe) with power of 10 mW. Since the Gd-PAN complex absorbs strongly in 525 – 575 nm spectral region, the 532 nm green laser (10 mW) was than utilized for excitation beam purposes. On the other hand, the complex compound Gd-PAN does not absorb the light at 660 nm and thus, by decreasing of light intensity from 660 nm laser, by a neutral density filter, it could be used as a probe beam source. For the all TLM measurements, quartz cuvette with 2 mm optical pathlength was used.

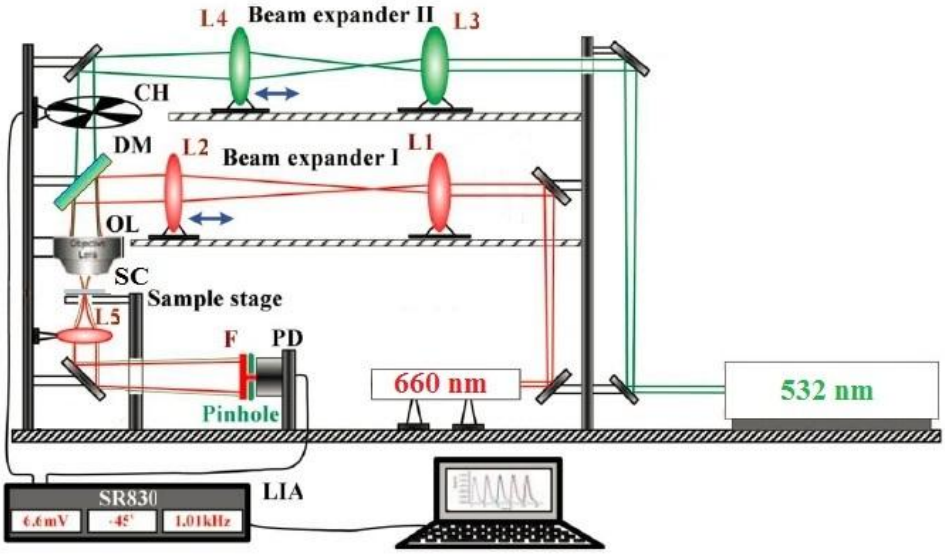

Figure 22. Schematic diagram of our TLM system. CH: mechanical chopper; DM: dichroic mirror; F: interference filter; L1 – L5: lenses; SC: sample cell; OL: objective lens; PD: photodiode; [161]

5.8.3 Total organic carbon

For the non-purgeable organic carbon (NPOC) and total nitrogen (TN) determination, AG MULTI N/C 3100 (Analytic Jena) instrument was used.

Approximately 25 mL of each sample was added into glass vials and placed into autosampler. Before first sample, 2 vials with deionized water were added to the sample rack to rinse the system and after each 3 samples, 1 vial with water was inserted. In Table 5, summarizes the method parameters. Before running the analysis, samples were manually acidified with 125 µL of 2 M HCl. In order to remove inorganic carbon, acidified samples were than purged with carbon-free air.

Table 5. TOC Analysis parameters

Method	NPOC-TN
Furnace	vertical
Furnace temperature	850°C
Rinse volume	2000 µL
Sample volume	500 µL
Repetitions	min.3, max.4
Variation coefficient	≥ 2%
Max. integration time	300s

5.8.4 Toxicity assessment

The toxicity tests were done accordingly to the OECD guidelines for testing of chemicals, test no. 202: *Daphnia sp.*; Acute Immobillisation Test [162]. All tests were done in 4 replicates, with 5 animals in 10 mL of aqueous media.

First, stock solutions of single substances (calcium chloride, magnesium sulfate, sodium bicarbonate, potassium chloride) were prepared accordingly to the ISO Test water (1) requirements.

Because of the low concentration of contaminant in the samples (in ultrapure water), we decided to double the recommended volumes, which should be added to deionized water in order to create artificial freshwater. This 2 times concentrated solution was afterwards diluted with our samples 1:1.

Second, the young *Dafnia magna* species were added to the vials with our samples in artificial freshwater, and placed on the table with day sunlight and constant temperature 20°C. After 48 hours, immobilized species were counted.

6. RESULTS AND DISCUSSION

The TLM and UV-Vis detection methods were used on the assumption that at one point, the Gd^{3+} ion will be released from the photocatalytically degraded compound. However, in degradation experiments desirable degradation efficiency was not achieved and thus, the reaction with ligand (PAN) was not detected. This could be caused by insufficient mineralization/release of gadolinium. For the samples from photoreactor, the products of complexation reaction with PAN were under the detection limits. The kinetics of degradation was followed by monitoring the dissolved organic carbon.

6.1 UV-Vis Spectrophotometry and thermal lens microscopy

6.1.1 Calibration

For calibration, stock standard solution of Gadolinium(III) nitrate hydrate with concentration 38.16 μM was prepared and subsequently diluted to achieve desired gadolinium concentration. Measurements within the concentration range from 1.9 μM (300 μg/L) to 38.16 μM (6 mg/L) were conducted.

6.1.2 UV-Vis spectrophotometry

Calibration measurements were conducted with respect to the blank, which consisted of given volume of reagent solution in surfactant (described above) and respective amount of deionized water, in 10 mm quartz cell.

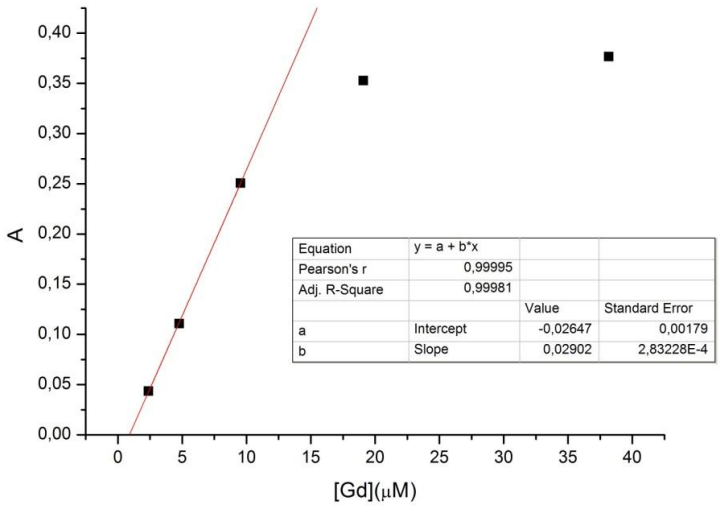

Figure 23. Calibration curve for Gd-PAN complex, done at λ = 532 nm with UV-Vis spectrophotometer.

For all measurements the same blank (c_{PAN} = 0.12 mM, c_{CTAB} = 0.2 mM) was used, and this had a great influence on the measurements at higher concentrations. The higher gadolinium concentration, the lower concentration of free ligand in the solution and thus, only one blank value for subtraction is not appropriate. For low concentration of Gd, the blank changes are negligible, and therefore the calibration curve is linear.

From calibration line, the limit of detection is calculated as a three times the standard deviation of the blank signal (n=10) (SD_{blank}) divided by the slope of the calibration curve (b):

$$LOD = \frac{3SD_{blank}}{b} \qquad (6.1)$$

The standard deviation of blank sample was SD_{blank}= 9.17x 10^{-4}, and the slope of calibration curve was 0.0292/μM. LOD was than calculated to be 0.1 μM which represents the amount of 15.7 μg/L of gadolinium. Limit of quantification (LOQ) was calculated similarly (eq.5.5) to be 0.31 μM (48.7 μg/L).

$$LOQ = \frac{10SD_{blank}}{b} \qquad (6.2)$$

The achieved LOD compares favorably to the results reported in literature [160] where an LOD of 0.8 μM can be calculated from the reported molar absorptivity of 7.9 L/mol.cm.

6.1.3 Thermal lens microscopy

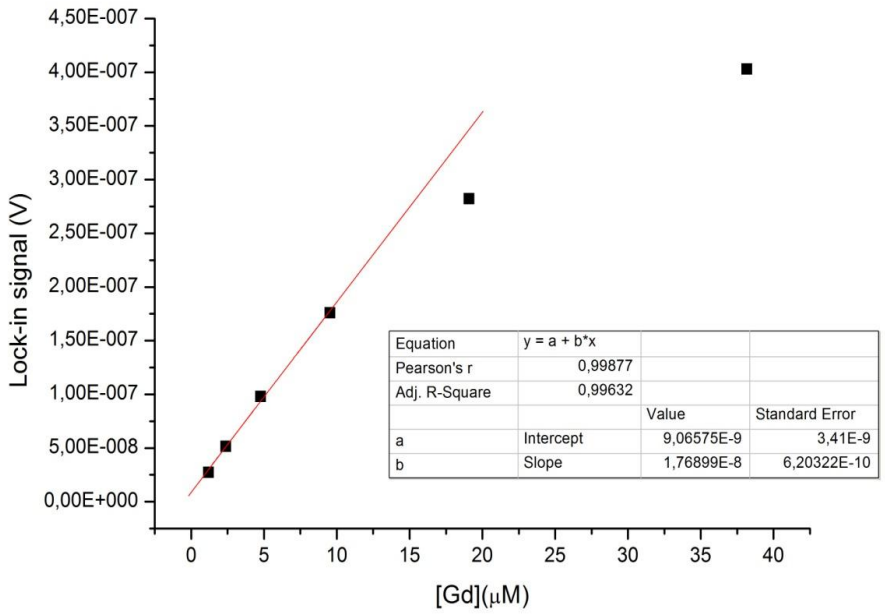

Figure 24. Calibration curve for Gd-PAN complex, measured by TLM system.

The measurements were done in 2 mm quartz cell. The LOD and LOQ was calculated analogically to UV-Vis method (eq. 5.1 and 5.2). For SD_{blank} = 2.4 x 10^{-9} V, and calibration line slope b= 1.7689x10^{-8} V/μM, LOD is 0.4 μM (62.9 μg/L of gadolinium) and LOQ = 1.36 μM (213.9 μg/L of gadolinium).

From the theory of TLS [117-119, 121] we can predict a simmilar sensitivity of TLS and spectrophotometry for a 10 mW excitation power, while 100 mW power would provide a 10 times better sensitivity. Considering only a 2 mm optical pathlength in case of TLM measurements, the LOD of 0.4 μM for TLM is in good agreement with LOD of 0.1 μM for spectrophotometry, what confirms quality of alignment and optimization of the TLM instrument.

6.1.4 Sample measurements

The samples which were taken during the degradation experiments, were not reacting with PAN reagent solution and thus, it was impossible to detect any signs of degradation. We assume, that this can be caused by the insufficient degradation of pollutant. Obviously, gadolinium atoms are still bonded with some parts of the original compound and the chealting power of PAN is too low to make complexation reaction possible, or the gadolinium release from the original complex was smaller than LOD value (0.1μM).

6.2 Total organic carbon

6.2.1 Ozonation experiments

Non-purgeable organic carbon (NPOC), total nitrogen (TN), pH measurement results, as well as degradation curve data and ln(c_0/c) are summarized in Tab.6. The graphical visualization can be seen as well.

Table 6. Results of NPOC, TN and pH measurements for ozonation experiments

Ozonation						
Time[hr]	**NPOC [mg/L]**	**TN [μg/L]**	**pH**	**c/c0**	**ln(c_0/c)**	**1/c [(mg/L)$^{-1}$]**
0	6.86	331.9	4.37	1	0	0.146
0.5	4.55	366.9	4.20	0.663	0.411	0.220
1	2.97	340.7	4.27	0.433	0.837	0.337
2	2.70	398.2	4.21	0.396	0.932	0.370
3.5	2.49	444.2	4.22	0.363	1.013	0.402

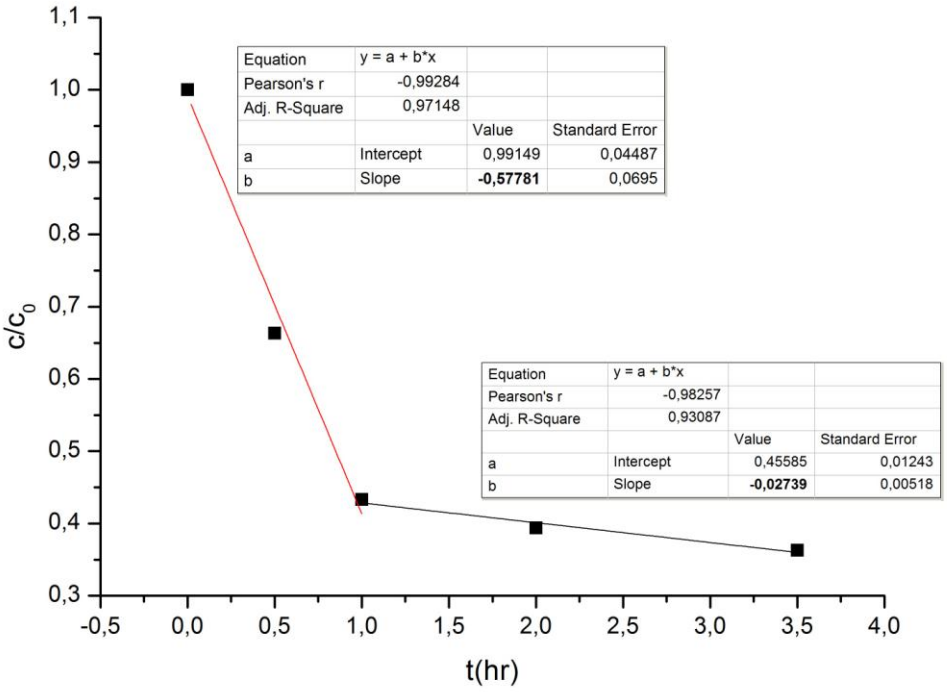

Figure 25. The zero-order kinetics plots

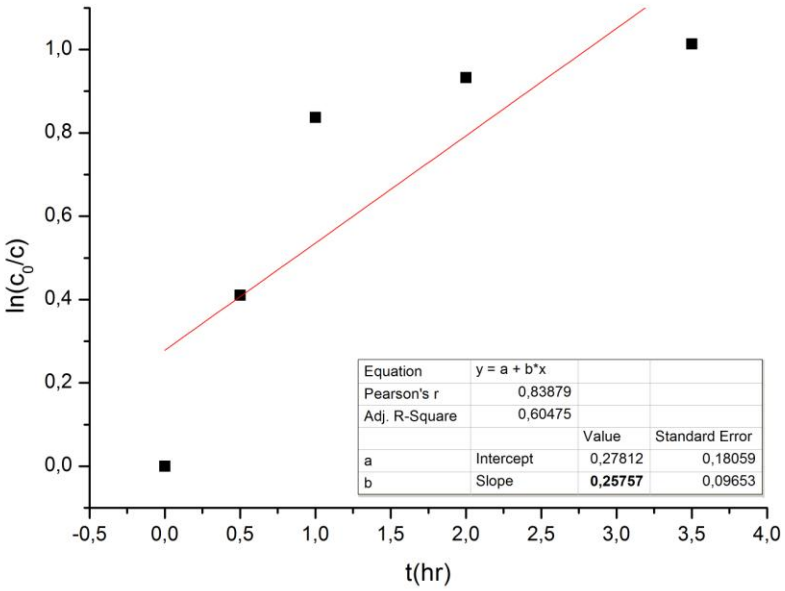

Figure 26. The first-order kinetics plot

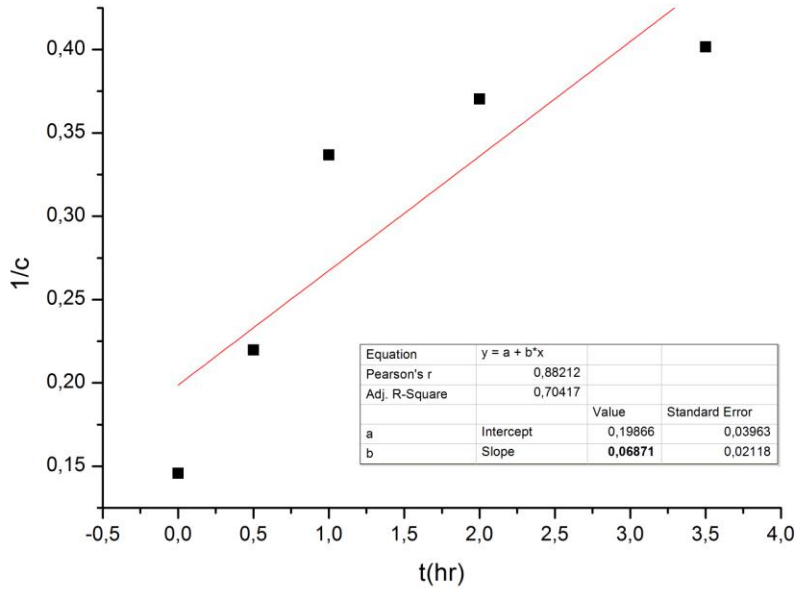

Figure 27. The second-order kinetics plot

6.2.2 Photocatalysis experiments

Non-purgeable organic carbon (NPOC), total nitrogen (TN), pH measurement results as well as degradation curve and $\ln(c_0/c)$ are summarized in Tab.7. The graphical visualization can be seen as well.

Table 7. Results of NPOC, TN and pH measurements for photocatalytic degradation experiments

TiO2						
time	**NPOC [mg/L]**	**TN [mg/L]**	**pH**	**c/co**	**$\ln(c_0/c)$**	**1/c $[(mg/L)^{-1}]$**
0	9.17	1.77	6.89	1	0	0.109
0.5	6.01	1.20	6.80	0.655	0.423	0.166
1	3.45	1.09	5.15	0.376	0.978	0.290
2	2.28	1.36	6.62	0.249	1.392	0.439
3.5	1.20	1.08	6.63	0.131	2.034	0.833

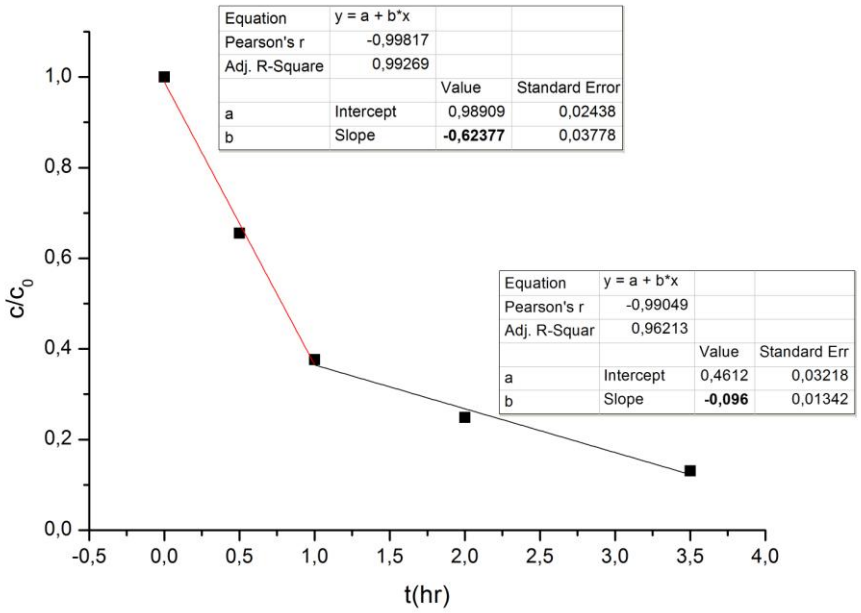

Figure 28. The zero-order kinetics plots

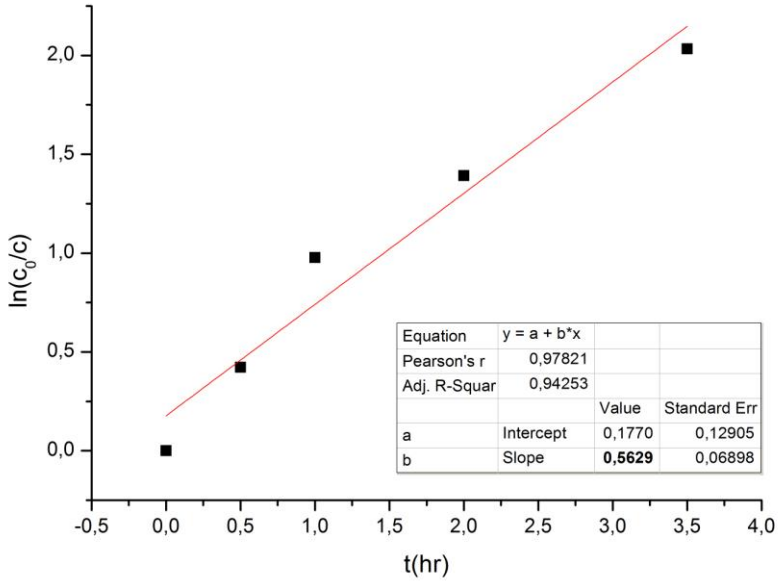

Figure 29. The first-order kinetics plot

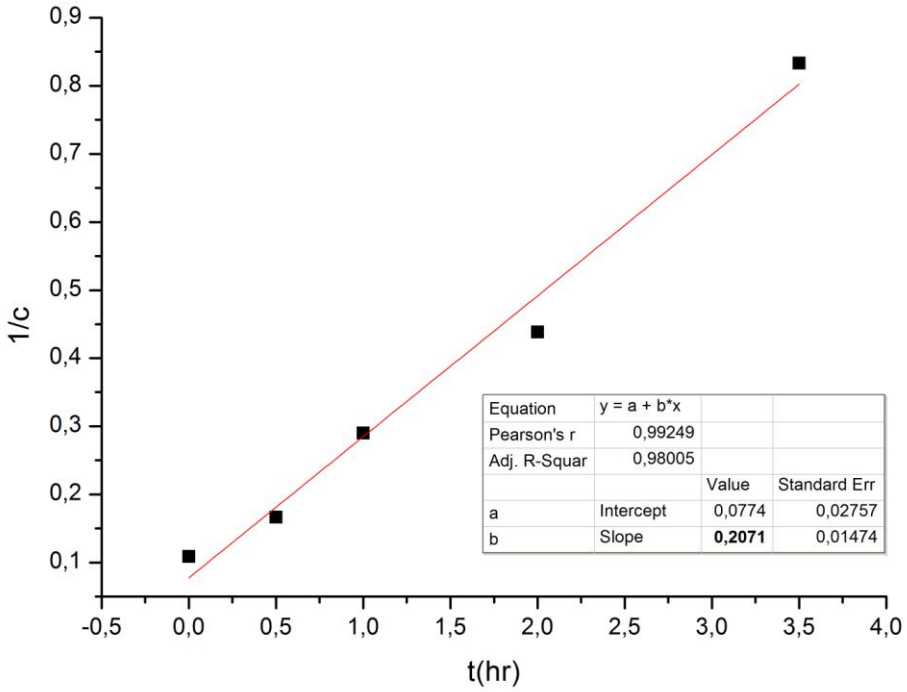

Figure 30. The second-order kinetic plot

6.2.3 Reaction kinetics

6.2.3.1 Ozonation

The reaction rate of degradation by ozone, in our system was best fitted by linear equations (Fig.25), which are describing the pseudo-zero-order reactions. The other 2 plots (Fig.26 and 27) are showing, that the reaction rate order of mineralization is most likely not of the first, nor the second order. If it would be so, the correlations (Fig.26 and27) would have to be linear. In the first one hour of degradation, we can see relatively rapid mineralization where 66% of the initial TOC for ozonation and 63% for photocatalysis is mineralized. A zero-order occurs when the reaction rate is constant during the whole period of experiment. This can happen when the concentration reduction per time is negligible with respect to the initial or remaining concentration. This kind of kinetics is always an artifact of the experimental conditions. Because of this, reactions following zero-order are often called as pseudo-zero-order reactions. A zero-order process can not be continuous until the whole pollutant dose is degraded. Before this point is reached, the reaction switches to another rate order. However, we need to keep in mind that in our case, we are talking about the mineralization rate and not the gadobutrol degradation rate. Zero-order reactions can be described as:

$$c = c_0 - kt \qquad (6.3)$$

Where c_0: relative initial concentration (c_0 = 100%); c: instantaneous concentration; k: rate constant; t: time. From the correlation of pollutant concentration and the irradiation time we can get the rate constant k. This correlation has a linear character, and k is the slope of the mathematical equation of this line. There are however 2 lines for each degradation method. For the next calculations of half-life we will use the rate constants of both. Rate constants obtained from our experimental data and half-life times are in the Table 8. Half-life was calculated as:

$$t_{1/2} = \frac{c_0}{2|k|} \qquad (6.4)$$

Table 8. Obtained pseudo-zero-order rate constants and calculated 1st half-life times.

	ozonation	photocatalysis
k-1 (hr^{-1})	0.578	0.624
k-2 (hr^{-1})	0.027	0.096
$t_{1/2}$-*1*(hr)	0.865	0,802
$t_{1/2}$-*2*(hr)	7.407	2,083

Where: k-1; $t_{1/2}$-1; are the rate constants and half-life times (c_0 = 100%) for the first 1 hour of experiment; and: k-2; $t_{1/2}$-2 are the rate constants and half-life times (c_0 = 40%) for the remaining duration of experiment.

6.2.3.2 Photocatalysis

The reaction rate of photocatalysis, can be described better by pseudo-second-rate order, when considering the plotting among the rest. This can be assumed due to good linearity (R^2 = 0.98) of correlation between 1/c and the time (Fig.30). However, there are some similarities with the ozonation – reaction rate becomes lower after certain point (1 hour), which would be normal for the first-order and the second-order reactions but not for the zero-order reactions. Calculation of the mineralization half-life times for both, pseudo-first and pseudo-second order was done as follows:

- Pseudo-first order $t_{1/2} = \ln 2/k$, for k = 0.563 h^{-1}, $t_{1/2}$ = 1.23h
- Pseudo-second order $t_{1/2} = 1/(k.c_0)$, for k = 0.207 h^{-1}, $t_{1/2}$ = 4.83h

The half-life differs for different kinetics: (i) for zero-order every next half-life is shorter; (ii) for first-order the half-life remains constant; (iii) for second-order it is getting longer.

6.2.3.3 Summary

From the computed half-life times, we can see that the most inaccurate is the second-order model even though our data fits graphically better than into the first-order kinetics model. The first-order kinetic constant predicts mineralization by 87.5% in 3.7 hours which is close to our experimental data (83% in 3.5hr). Nonetheless, it is not corresponding with the first one hour of experiment (same as the second-order kinetics), where the mineralization goes faster than expected from the first-order kinetics model. The overall mineralization kinetics is then very difficult to summarize by one kinetics model, and for the ozonation, based on the data obtained, even harder.

Nevertheless, what we assume, is that during the mineralization many degradation products are created which are following different kinetic models. The beginning of mineralization is relatively fast. Approximately 65% of the total organic carbon (TOC) removal in 1 hour may be caused by the decarboxylation and dealkylation of the carbon atoms, which are not the part of a 1,4,7,10-Tetraazocyclododecane core of the ligand. This core is consisting of 8 carbon atoms, which are representing about 45% of TOC in the molecule. However, this is just a speculation and we would need different techniques, such as mass spectroscopy to follow the degradation.

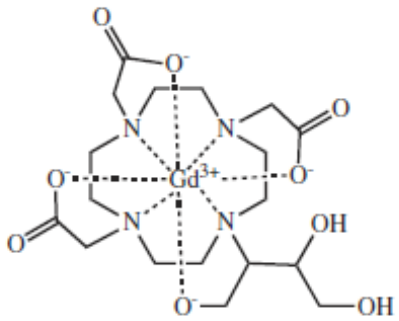

Gd-BT-DO3A
(Gadovist®)

Figure 31. Structure of mother compound

6.3 Toxicity assessment

After 48 hours, following immobilization counts were recorded:

Table 9. Counts of non-immobilized *daphnias*, for ozonation experiments. ($\cancel{O}_3$ means no ozone = blank)

No.of vial	control	$\cancel{O}_3$ 0min	O_3 0hr	O_3 0,5hr	O_3 1hr	O_3 2hr	O_3 3,5hr	O_3 5hr
1	5	5	5	5	5	5	3	5
2	5	5	4	4	5	5	5	5
3	5	5	4	5	4	5	5	5
4	5	5	5	4	4	5	4	4
Immobilization rate (%)	0	0	10	10	10	0	15	5

Table 10. Counts of non-immobilized *daphnias*, for photocatalysis experiments.

No. Of vial	control	0hr	0,5hr	1hr	2hr	3,5hr	5hr
1	4	5	4	3	4	5	5
2	5	4	1	5	5	5	5
3	5	5	3	3	5	5	5
4	5	5	3	5	4	5	5
Immobilization rate (%)	5	5	45	20	10	0	0

From the obtained data, it is difficult to find any trend, or make some conclusions. Nevertheless, the non-degraded contaminant seem to be less toxic than it's degradation products.

6.4 Desorption experiments

After discovering the fact, that there are no free Gd ions in the solution, the desorption experiments were carried out. Fresh catalyst slides were prepared, and each of them was used only once. After the end of degradation experiment, slide was submerged into 50 mL of 0.1M sodium hydroxide solution and purged by air to ensure the mixing for 1 hour. The solution was than neutralized by 0.1M hydrochloric acid, and then tested for the presence of gadolinium ions. The results were negative, which indicates that the surface absorption is probably not the reason why the metal is not in the solution after degradation.

7. CONCLUSION

For degradation experiments of commercially available magnetic resonance imagining contrast agent gadobutrol (Gd-BT-DO3A or Gadovist®), titanium dioxide Aeroxide® P25 (80% Anatase, 20% Rutile) was succesfully immobilized on the glass slides surface employing sol-gel method. The direct detection of analyte was not possible due to the lack of light absorption in the visible light and UVA spectrum. Spectrometric method based on the complexation reaction of gadolinium ions with 1-(2-Pyridylazo)-2-naphtol (PAN) ligand was utilized for mineralization rate determination. Beer-Lambert law was studied over the concentration range from 1.9 μM (300 μg/L) to 38.16 μM (6 mg/L). The correlation between concentration and signal was observed to be linear for both, UV-Vis spectrophotometry and thermal lens microscope in the range between 1.9 μM and 10 μM. The limits of detection were calculated to be 0.1 μM and 0.4 μM for the spectrophotometry and thermal lens microscopy respectively. Thermal lens techniques are known for their high sensitivity, which is directly proportional to the pump beam power. Laser power of utilized pump beam in the improvised TLM system, was relatively low (10 mW) and this fact affected the LOD value significantly. Another reason for higher LOD is the difference in optical length of cuvette, which was 5 times shorter when compared to spectrofotometric determination. However, total mineralization and the gadolinium ions released from the mother compound were below the limits of detection. The metal adsorption onto catalyst's surface was not confirmed. For this purpose, ozonation was implemented and also desorption experiments with used slides were conducted. The kinetics of degradation was after followed by the non-purgeable organic carbon measurements. Degradation efficiencies were: (i) photocatalysis (87% TOC decrease within 3 hours), assisted by TiO_2 and UVA light, and (ii) ozonation (72% TOC decrease within 3 hours), assisted only by O_3. Toxicity tests with *Dafnia magna* revealed, that the degradation products are most likely more toxic than the mother compound and thus, it is debatable whether it is necessary to degrade it, or not.

The method employing 1-(2-Pyridylazo)-2-naphtol as a colorimetric reagent is very sensitive and non-selective (reaction runs with most of transition metals). Probably the most suitable technique for degradation monitoring of Gd-based contrast agents, also in the real samples is HILIC chromatography with mass spectrometric detection.

8. REFERENCES

[1] FUJISHIMA, A.; HONDA, K.: Electrochemical Photolysis of Water at a Semiconductor Electrode. *Nature*. 1972, **1972**(238), 37-38. DOI: 10.1038/238037a0.

[2] FUJISHIMA, A.; ZHANG, X.; TRYK, D.: TiO2 photocatalysis and related surface phenomena. *Surface Science Reports*. 2008, **63**(12), 515-582. DOI: 10.1016/j.surfrep.2008.10.001. ISSN 01675729.

[3] HENDERSON, M.: A surface science perspective on TiO2 photocatalysis. *Surface Science Reports*. 2011, **66**(6-7), 185-297. DOI: 10.1016/j.surfrep.2011.01.001. ISSN 01675729.

[4] HOIGNE, J.: Inter-calibration of oh radical sources and water quality parameters. *Water Science and Technology*. 1997, **35**(4), 1-8. DOI: 10.1016/S0273-1223(97)00002-4. ISSN 02731223.

[5] RIBEIRO, R.; NUNES, O.; PEREIRA, M.; SILVA, A.: An overview on the advanced oxidation processes applied for the treatment of water pollutants defined in the recently launched Directive 2013/39/EU. *Environment International*. 2015, **75**, 33-51. DOI: 10.1016/j.envint.2014.10.027. ISSN 01604120.

[6] RAUF, A.; ASHRAF, S.: Fundamental principles and application of heterogeneous photocatalytic degradation of dyes in solution. *Chemical Engineering Journal*. 2009, **151**(1-3), 10-18. DOI: 10.1016/j.cej.2009.02.026. ISSN 13858947

[7] PATTANAIK, P.; SAHOO, M.K.: Desalination and Water Treatment. 2014, **52** (34-36), 6567-6590. DOI: 10.1080/19443994.2013.822187. ISSN 1944-3994.

[8] Structure of TiO_2 crystals. Figures available at University of Colorado website - http://ruby.colorado.edu/~smyth/min/tio2.html ; last modified on Sep. the 7th 2015.

[9] CHONG, M.N.; JIN, B.; CHOW, CH.; SAINT, CH.: Recent developments in photocatalytic water treatment technology: A review. *Water Research*. 2010, **44**(10), 2997-3027. DOI: 10.1016/j.watres.2010.02.039. ISSN 00431354.

[10] CARP, O.; HUISMANN, C.L.; RELLER, A.: Photoinduced reactivity of titanium dioxide. *Progress in Solid State Chemistry*. 2004, 32(1-2):33-177. DOI: 10.1016/j.progsolidstchem.2004.08.001

[11] LINSEBIGLER, A.L.; LU, G.; YATES, J.T.Jr.: Photocatalysis on TiO_2 Surfaces: Principles, Mechanisms, and Selected Results. *Chemical Reviews*. 1995, 95(3):735-758.

[12] FURUBE, A.; ASAHI, T.; MASUHARA, H.; et. al.: Direct observation of a picosecond charge separation process in photoexcited platinum-loaded TiO2 particles by femtosecond diffuse reflectance spectroscopy. *Chemical Physics Letters*. 2001, **336**(5-6), 424-430. DOI: 10.1016/S0009-2614(01)00128-2. ISSN 00092614.

[13] BYRNE, J.A.; Eggins, B.R.: Photochemistry of oxalate on particulate TiO_2 electrodes. *Journal of Electroanalytical chemistry,* 1998, 457, 61-72.

[14] FOGLER, H.S., 1999. *Elements of Chemical Reaction Engineering*: Chapter 10: Catalysis and Catalytic Reactors. Prentice-Hall PTR Inc, p. 581 - 685.

[15] VINODGOPAL, K.; KAMAT, P.: Photochemistry on surfaces: photodegradation of 1,3-diphenylisobenzofuran over metal oxide particles. *The Journal of Physical Chemistry*. 1992, **96**(12), 5053-5059. DOI: 10.1021/j100191a058. ISSN 0022-3654.

[16] HERRMANN, J. M.: Heterogeneous photocatalysis: state of the art and present applications. *Topics in Catalysis*. 2005, **34**(1-4), 49-65.
DOI: 10.1007/s11244-005-3788-2. ISSN 1022-5528.

[17] HERRMANN, J. M.; PICHAT, P.; et. al.: Photocatalytic hydrogen-production from aliphatic-alcohols over bifunctional platinum on titanium-dioxide catalyst. *New Journal of Chemistry.* 1981, 5(12), 627-636. ISSN 0398-9836.

[18] KONSTANTINOU, I. K.; ALBANIS, T.: TiO2-assisted photocatalytic degradation of azo dyes in aqueous solution: kinetic and mechanistic investigations. *Applied Catalysis B: Environmental*. 2004, **49**(1), 1-14.
DOI: 10.1016/j.apcatb.2003.11.010. ISSN 09263373.

[19] POULIOS, I., TSACHPINIS, J.:Photodegradation of the textile dye Reactive Black 5 in the presence of semiconducting xides. *Journal of chemical technology and biotechnology*. 1997, 74(4), 349-357.

[20] TUNESI, S.; ANDERSON. M.: Influence of chemisorption on the photodecomposition of salicylic acid and related compounds using suspended titania ceramic membranes. *The Journal of Physical Chemistry* . 1991, **95**(8), 3399-3405. DOI: 10.1021/j100161a078. ISSN 0022-3654.

[21] FOX, M.A; DULAY, M.T.: Heteroheneous Photocatalysis, *Chem. Rev.* 1993, 93, 341-357.

[22] IRMAK, S.; KUSVURAN, E.: Degradation of 4-chloro- 2-methylphenol in aqueous solution by UV irradiation in the presence of titanium dioxide.
Appl. Catal. B: Environ. 2004, 54, 85–91.

[23] RAVICHANDRAN, L.; SELVAM, K.: Effect of oxidants and metal ions on photodefluoridation of pentafluorobenzoic acid with ZnO. *Sep. Purif. Technol*.
2007, 56, 192–198.

[24] SELVAM, K.; MURUGANANDHAM, M.; et al.: The influence of inorganic oxidants and metal ions on semiconductor sensitized photodegradation of
4-fluorophenol. *Chem. Eng. J*. 2007, 128, 51–57.

[25] MALATO, S.; BLANCO, J.; et al.: Enhancement of the rate of solar photocatalytic mineralization of organic pollutants by inorganic oxidizing species.
Appl. Catal. B: Environ. 1998, 17, 347–356.

[26] DOGLIOTTI, L.; HAYON, E.: Flash photolysis of peroxydisulfate ions in aqueous solutions. The sulfate and ozonide radical anions. *J. Phys. Chem*. 1967, 71, 2511–2516.

[27] SADIK, W.A.; SADEK, O.M.; et al.: The use of heterogeneous advanced oxidation processes to degrade neutral red dye in aqueous solution. *Polym. Plast. Technol. Eng.* 2004, 43, 1675–1686.

[28] WANG, Y.; HONG, C.: Effect of hydrogen peroxide, periodate and persulfate on photocatalysis of 2-chlorobiphenyl in aqueous TiO2 suspensions. *Water Res*. 1999, 33, 2031–2036.

[29] LEE, C.; YOON, J.: Application of photoactivated periodate to the decolorization of reactive dye: Reaction parameters and mechanism. *J. Photochem. Photobiol. A: Chem*. 2004, 165, 35–41.

[30] SADIK, W.A.: Effect of inorganic oxidants in photodecolourization of an azo dye. *J.Photochem. Photobiol. A: Chem.* 2007, 191, 132–137.

[30] ZHANG, L.; DILLERT, R,; et al.: Photo-induced hydrophilicity and self-cleaning:models and reality. *Energy Environ Sci.* 2012, 5, 7491–7507.

[31] AKLY, C.; CHADIK, P.A.; MAYZCK D.W.: Photocatalysis of gas-phase toluene using silica-titania composites: performance of a novel catalyst immobilization technique suitable for large-scale applications. *Appl Catal B Environ*. 2010, 99, 329–335.

[32] FOLLI, A.; PADE, C.; HANSEN, T.B.; et al.: TiO2 photocatalysis in cementitious systems: insights into self-cleaning and depollution chemistry. *Cem Concr Res*. 2012, 42, 539–548.

[33] TASBIHI, M.; KETE, M.; RAICHUR, A.M.; et al: Photocatalytic degradation of gaseous toluene by using immobilized titania/silica on aluminum sheets. *Environ Sci Pollut Res.* 2012, 19, 3735–3742.

[34] ZHU, X.; NANNY, M.A.; BUTLER, E.C.: Photocatalytic oxidation of aqueous ammonia in model gray waters. *Water Res*. 2008, 42, 2736–2744.

[35] MIRANDA-GARCIA, N.; MALDONADO, M.I.; et al.: Degradation study of 15 emerging contaminants at low concentration by immobilized TiO2 in a pilot plant. *Catal Today. 2010*, 151, 107–113.

[36] SANCHEZ,M.; RIVERO, M.J.; ORTIZ, I.: Photocatalytic oxidation of grey water over titanium dioxide suspensions. *Desalination*. 2010, 262, 141–146.

[37] MALATO, S.; FERNANDEZ-IBANEZ, P.; MALDONADO, M.I.; et al.: Decontamination and disinfection of water by solar photocatalysis: recent overview and trends. *Catal Today*. 2009, 147, 1–59.

[38] RIZZO, L.: Inactivation and injury of total coliform bacteria after primary disinfection of drinking water by TiO2 photocatalysis.
J Hazard Mater. 2009, 165, 48–51.

[39] SCIACCA, F.; RENGIFO-HERRERA, J.A,; WETHE, J.; PULGARIN, C.: Solar disinfection of wild salmonella sp. in natural water with a 18 L CPC photoreactor: detrimental effect of non-sterile storage of treated water.
Sol Energy. 2011, 85, 1399–1408.

[40] IMOBERDORF, G.E.; VELLA, G.; SCLAFANI, A.; et al.: Radiation model of a TiO2-coated, quartz wool, packed-bed photocatalytic reactor.
AIChE J. 2010, 56, 1030‐1044.

[41] KETE, M.; PAVLICA, E.; FRESNO, F.; et al.: Highly active photocatalytic coatings prepared by a low-temperature method. *Environmental Science and Pollution Research*. 2014, **21**(19), 11238-11249.

[42] LACOMBE, S.; KELLER, N.; Photocatalysis: fundamentals and applications in JEP 2011. *Environmental Science and Pollution Research*. 2012, **19**(9), 3651-3654.
DOI: 10.1007/s11356-012-1040-8. ISSN 0944-1344.

[43] FUJISHIMA, A.; RAO, T.; TRYK, R.: Titanium dioxide photocatalysis. *Journal of Photochemistry and Photobiology C: Photochemistry Reviews 1*. 2000, 1-21.

[44] FUJISHIMA, A.; ZHANG, X.: Titanium dioxide photocatalysis: present situation and future approaches. *Comptes Rendus Chimie*. 2006, **9**(5-6), 750-760.
DOI: 10.1016/j.crci.2005.02.055. ISSN 16310748.

[45] SUNADA, K.; KIKUCHI, Y.; et al.: Bactericidal and detoxification effects of TiO2 thin film photocatalysts. *Environ. Sci. Technol*. 1998, 32, 726–728.

[46] BLAKE, D.; MANESS, P.; et al.: Application of the photocatalytic chemistry of titanium dioxide to disinfection and the killing of cancer cells. *Separation and Purification Methods*. 1999, 28(1), 1-50.

[47] LAUFFER, R.B.: Paramagnetic metal-complexes as water proton relaxation agents for NMR Imaging-theory and design. *Chem Rev.* 1987, 87, 901–927.

[48] CARAVAN, P.; ELLISON, J.J.; MCMURRY, T.J.; LAUFFER, R.B.: Gadolinium(III) chelates as MRI contrast agents: structure, dynamics, and applications. *Chem Rev.* 1999, 99, 2293–2352.

[49] ZHOU, Y.; LU, Z-R.: Gadolinium-based contrast agents for magnetic resonance cancer imaging. *WIREs Nanomed. Nanobiotechnol*. 2013, 5, 1-18. DOI: 10.1002/wnan.1198

[50] DAMADIAN, R.: Tumor detection by nuclear magnetic resonance. *Science.* 1971, 171, 1151–1153.

[51] SHOKROLLAHI, H.: Contrast agents for MRI. *Materials Science and Engineering: C*. 2013, **33**(8), 4485-4497. DOI: 10.1016/j.msec.2013.07.012. ISSN 09284931

[52] SCHNECK, J.F.: The role of magnetic susceptibility in magnetic resonance imaging: MRI magnetic compatibility of the first and second kinds. *Med. Phys.* 1996, 23, 815.

[53] NA, H. B.; SONG, I.CH.; HYEON, T.: Inorganic Nanoparticles for MRI Contrast Agents. *Advanced Materials*. 2009, **21**(21), 2133-2148. DOI: 10.1002/adma.200802366. ISSN 09359648.

[54] BIANCHI, A,; CALABI, L.; et al.: Thermodynamic and structural properties of Gd (III) complexes with polyamino-polycarboxylic ligands: basic compounds for the development of MRI contrast agents.*Coordination Chemistry Reviews*. 2000, **204**(1), 309-393. DOI: 10.1016/S0010-8545(99)00237-4. ISSN 00108545

[55] CHINTHALAPATI, S. K. R, SCHARF, H.; JAKUBOWSKI, N.; PANNE, U.: A novel solid phase extraction method for pre-concentration of gadolinium and gadolinium based MRI contrast agents from the environment. *Journal of Analytical Atomic Spectrometry*. 2010, **25**(10), 1573-1580. DOI: 10.1039/c003251d. ISSN 0267-9477.

[56] TELGMANN, L.; SPERLING, M.; KARST, U.: Determination of gadolinium-based MRI contrast agents in biological and environmental samples: A review. *Analytica Chimica Acta*. 2013, **764**, 1-16. DOI: 10.1016/j.aca.2012.12.007. ISSN 00032670.

[57] KNAPPE, A.; MÖLLER, P.; DULSKI, P.; PEKDEGER, A.: Positive gadolinium anomaly in surface water and ground water of the urban area Berlin, Germany. *Chemie der Erde - Geochemistry*. 2005, **65**(2), 167-189. DOI: 10.1016/j.chemer.2004.08.004. ISSN 00092819.

[58] BAU, M.; DULSKI, P.: Anthropogenic origin of positive gadolinium anomalies in river waters. *Earth and Planeary Science Letters*. 1996, 143, 245–255.

[59] MERSCHEL, G.; BAU, M.: Rare earth elements in the aragonitic shell of freshwater mussel Corbicula fluminea and the bioavailability of anthropogenic lanthanum, samarium and gadolinium in river water. *Science of The Total Environment*. 2015, **533**, 91-101.DOI: 10.1016/j.scitotenv.2015.06.042. ISSN 00489697.

[60] BAU, M.; KNAPPE, A.; DULSKI, P.: Anthropogenic gadolinium as a micropollutant in river waters in Pennsylvania and in Lake Erie, northeastern United States. *Chemie der Erde - Geochemistry*. 2006, **66**(2), 143-152. DOI: 10.1016/j.chemer.2006.01.002. ISSN 00092819.

[61] LAWRENCE, M.G.: Detection of anthropogenic gadolinium in the Brisbane River plume in Moreton Bay, Queensland, Australia. *Marine Pollution Bulletin* . 2010, **60**(7), 1113-1116. DOI: 10.1016/j.marpolbul.2010.03.027. ISSN 0025326x.

[62] MÖLLER, P.; PACES, T.; DULSKI, P.; MORTEANI, G.: Anthropogenic Gd in Surface Water, Drainage System, and the Water Supply of the City of Prague, Czech Republic. *Environmental Science & Technology*. 2002, **36**(11), 2387-2394. DOI: 10.1021/es010235q. ISSN 0013-936x.

[63] KÜMMERER, K.; HELMERS, E.: Hospital Effluents as a Source of Gadolinium in the Aquatic Environment. *Environmental Science & Technology*. 2000, **34**(4), 573-577. DOI: 10.1021/es990633h. ISSN 0013-936x.

[64] KÜNNEMEYER, J.; TERBORG, L.; MEERMANN, B.; BRAUCKMANN.; et al.:Speciation Analysis of Gadolinium Chelates in Hospital Effluents and Wastewater Treatment Plant Sewage by a Novel HILIC/ICP-MS Method. *Environmental Science & Technology*. 2009, **43**(8), 2884-2890. DOI: 10.1021/es803278n. ISSN 0013-936x.

[65] RABIET, M.; BRISSAUD, F.; SEIDEL, J.L.; PISTRE, C.; et al.: Positive gadolinium anomalies in wastewater treatment plant effluents and aquatic environment in the Hérault watershed (South France). *Chemosphere*. 2009, **75**(8), 1057-1064. DOI: 10.1016/j.chemosphere.2009.01.036. ISSN 00456535.

[66] MÖLLER, P.; ROSENTHAL, E.; DULSKI, P.; et al.: Rare earths and yttrium hydrostratigraphy along the Lake Kinneret–Dead Sea–Arava transform fault, Israel and adjoining territories. *Applied Geochemistry*. 2003, **18**(10), 1613-1628. DOI: 10.1016/S0883-2927(03)00044-1. ISSN 08832927.

[67] MERSCHEL, G; BAU, M.; BALDEWEIN, L.; et al.: Tracing and tracking wastewater-derived substances in freshwater lakes and reservoirs: Anthropogenic gadolinium and geogenic REEs in Lake Paranoá, Brasilia. *Comptes Rendus Geoscience*. 2015, **347**(5-6), 284-293. DOI: 10.1016/j.crte.2015.01.004. ISSN 16310713.

[68] KLAVER, G.; VERHEUL, M.; BAKKER, I.; et al.: Anthropogenic Rare Earth Element in rivers: Gadolinium and lanthanum. Partitioning between the dissolved and particulate phases in the Rhine River and spatial propagation through the Rhine-Meuse Delta (the Netherlands).*Applied Geochemistry*. 2014, **47**, 186-197. DOI: 10.1016/j.apgeochem.2014.05.020. ISSN 08832927.

[69] KULAKSIZ, S.; BAU, M.: Contrasting behaviour of anthropogenic gadolinium and natural rare earth elements in estuaries and the gadolinium input into the North Sea. *Earth and Planetary Science Letters*. 2007, **260**(1-2), 361-371. DOI: 10.1016/j.epsl.2007.06.016. ISSN 0012821x.

[70] KULAKSIZ, S.; BAU, M.: Anthropogenic gadolinium as a microcontaminant in tap water used as drinking water in urban areas and megacities. *Applied Geochemistry*. 2011, **26**(11), 1877-1885. DOI: 10.1016/j.apgeochem.2011.06.011. ISSN 08832927.

[71] KULAKSIZ, S.; BAU, M.: Rare earth elements in the Rhine River, Germany: First case of anthropogenic lanthanum as a dissolved microcontaminant in the hydrosphere. *Environment International*. 2011, **37**(5), 973-979. DOI: 10.1016/j.envint.2011.02.018. ISSN 01604120.

[72] KULAKSIZ, S.; BAU, M.: Anthropogenic dissolved and colloid/nanoparticle-bound samarium, lanthanum and gadolinium in the Rhine River and the impending destruction of the natural rare earth element distribution in rivers. *Earth and Planetary Science Letters*. 2013, **362**, 43-50. DOI: 10.1016/j.epsl.2012.11.033. ISSN 0012821x.

[73] TELGMANN, L.; KARST, U.; et al.: Analysis of the Contrast Agent Magnevist and Its Transmetalation Products in Blood Plasma by Capillary Electrophoresis/Electrospray Ionization Time-of-Flight Mass Spectrometry. *Anal. Chem.*, 2009, 81 (9), 3600–3607. DOI: 10.1021/ac8027118.

[74] TELGMANN, L.; FABER, H.; et al: Identification and quantification of potential metabolites of Gd-based contrast agents by electrochemistry/separations/mass spectrometry. *Journal of chromatography*. 2012, 1240, 147-155.
DOI: 10.1021/ac8027118

[75] ABRAHAM, J.L.; CHANDRA, S.; THAKRAL, C.: SIMS imaging of gadolinium isotopes in tissue from Nephrogenic Systemic Fibrosis patients: Release of free Gd from magnetic resonance imaging (MRI) contrast agents. *Applied Surface Science*. 2008, **255**(4), 1181-1184. DOI: 10.1016/j.apsusc.2008.05.140. ISSN 01694332.

[76] ANDRÁSI, M.; GÁSPÁR, A.; et al.: Determination of gadolinium-based magnetic resonance imaging contrast agents by micellar electrokinetic capillary chromatography. *ELECTROPHORESIS*. 2011, **32**(16), 2223-2228.
DOI: 10.1002/elps.201100185. ISSN 01730835.

[77] ARBUGHI, T.; BERTANI, F.; et al.: High-performance liquid chromatographic determination of the magnetic resonance imaging contrast agent gadobenate ion in plasma, urine, faeces, bile and tissues. *Journal of Chromatography B: Biomedical Sciences and Applications*. 1998, **713**(2), 415-426.
DOI: 10.1016/S0378-4347(98)00190-X. ISSN 03784347.

[78] BEHRA-MILLET, J.; BRIAND, G.; et al.: On-line HPLC electrospray ionization mass spectrometry: a pharmacological tool for identifying and studying the stability of Gd3+ complexes used as magnetic resonance imaging contrast agents. *Biomedical Chromatography*. 1998, 12, 21-26.

[79] CACHERIS, W.P.; QUAY, C.; ROCKLAGE, S.: The relationship between thermodynamics and the toxicity of gadolinium complexes. *Magnetic Resonance Imaging*. 1990, **8**(4), 467-481. DOI: 10.1016/0730-725X(90)90055-7.
ISSN 0730725x.

[80] CAMPA, C.; ROSSI, M.; et al.: Analysis of gadobenate dimeglumine by capillary zone electrophoresis coupled with electrospray-mass spectrometry.
ELECTROPHORESIS. 2005, **26**(7-8), 1533-1540.
DOI: 10.1002/elps.200410111. ISSN 0173-0835.

[81] CHELLQUIST, E.; SEARLE, R.: An LC method for measuring complex formation equilibria by competitive chelation. *Journal of Pharmaceutical and Biomedical Analysis*. 1993, **11**(10), 985-992. DOI: 10.1016/0731-7085(93)80059-A. ISSN 07317085.

[82] ABRAHAM, J.L.; THAKRAL, C.; SKOV, L.; et al.: Dermal inorganic gadolinium concentrations: evidence for in vivo transmetallation and long-term persistence in nephrogenic systemic fibrosis. *British Journal of Dermatology*. 2008, **158**(2), 273-280. DOI: 10.1111/j.1365-2133.2007.08335.x. ISSN 00070963.

[83] ELBAZ-POULICHET, F.; SEIDEL, J-L.: Occurrence of an anthropogenic gadolinium anomaly in river and coastal waters of Southern France. *Water Research*. 2002,**36**(4), 1102-1105. DOI: 10.1016/S0043-1354(01)00370-0. ISSN 00431354.

[84] FRENZEL, T.; et al.: Stability of gadolinium-based magnetic resonance imaging contrast agent in human serum at 37 degrees C. *Investigative Radiology*. 2008, 43(12), 817-828.

[85] HAGAN, J.; TAYLOR, J.; TWEEDLE, M.: Fluorescence detection of gadolinium chelates separated by reversed-phase high-performance liquid chromatography. *Analytical Chemistry*. 1988, **60**(6), 514-516. DOI: 10.1021/ac00157a004. ISSN 0003-2700.

[86] HAUSTEIN, J.; SCHUHMANN-GIAMPIERI, G.. Elimination of Gd-DTPA by means of hemodialysis. *European Journal of Radiology*. 1990, **11**(3), 227-229. DOI: 10.1016/0720-048X(90)90064-I. ISSN 0720048x.

[87] HVATTUM, E.; NORMANN, P.; et al.: Detection and quantitation of gadolinium chelates in human serum and urine by high-performance liquid chromatography and post-column derivatization of gadolinium with Arsenazo III. *Journal of Pharmaceutical and Biomedical Analysis*. 1995, **13**(7), 927-932. DOI: 10.1016/0731-7085(95)01311-8. ISSN 07317085.

[88] JOFFE, P.; THOMSEN, H.; MEUSEL, M.: Pharmacokinetics of gadodiamide injection in patients with severe renal insufficiency and patients undergoing hemodialysis or continuous ambulatory peritoneal dialysis. *Academic Radiology*. 1998, **5**(7), 491-502. DOI: 10.1016/S1076-6332(98)80191-8. ISSN 10766332.

[89] KAHAKACHCHI, C.L.; MOORE, D.: Speciation of gadolinium in gadolinium-based magnetic resonance imaging agents by high performance liquid chromatography inductively coupled plasma optical emission spectrometry. *Journal of Analytical Atomic Spectrometry*. 2009, **24**(10), 1389- 1396. DOI: 10.1039/b907044c. ISSN 0267-9477.

[90] KÜNNEMEYER, J.; TERBORG, L.; NOWAK, S.; et al.: Speciation Analysis of Gadolinium-Based MRI Contrast Agents in Blood Plasma by Hydrophilic Interaction Chromatography/Electrospray Mass Spectrometry. *Analytical Chemistry* . 2008, **80**(21), 8163-8170. DOI: 10.1021/ac801264j. ISSN 0003-2700.

[91] KINDBERG, G.M.; URAN, S.; et al.: The fate of Gd and chelate following intravenous injection of gadodiamide in rats. *European Radiology*. 2010,**20**(7), 1636-1643. DOI: 10.1007/s00330-010-1716-8. ISSN 0938-7994.

[92] KÜNNEMEYER, J.; TERBORG, L.; NOWAK, S.; et al.: Quantification and excretion kinetics of a magnetic resonance imaging contrast agent by capillary electrophoresis-mass spectrometry. *Electrophoresis.* 2009, **30**(10), 1776-1773. DOI:10.1002/elps.2008-00831.

[93] KÜNNEMEYER, J.; TERBORG, L.; NOWAK, S.; et al.: Analysis of the contrast agent Magnevist and its transmetalation products in blood plasma by capillary electrophoresis/electrospray ionization time-of-flight mass spectrometry. *Analytical Chemistry*. 2009, **81**(9), 3600-3607. DOI: 10.1021/ac8027118.

[94] LAWRENCE, M.G.; KELLER, J.; et al.: Removal of magnetic resonance imaging contrast agents through advanced water treatment plants. *Water Science and Technology*. 2010, **61**(3), 685-692. DOI: 10.2166/wst.2010.885

[95] MORTEANI, G.; MÖLLER, P.; FUGANTI, A.: Input and fate of anthropogenic estrogens and gadolinium in surface water and sewage plants in the hydrological basin of Prague (Czech Republic). *Environmental Geochemistry and Health*. 2006,**28**(3), 257-264. DOI: 10.1007/s10653-006-9040-6. ISSN 0269-4042.

[96] LORETI, V.; BETTMER, J.: Determination of the MRI contrast agent Gd-DTPA by SEC-ICP-MS. *Analytical and Bioanalytical Chemistry*. 2004, **379**(7-8),1050-1054. DOI: 10.1007/s00216-004-2700-4. ISSN 1618-2642.

[97] LORUSSO, V.; POGGESI, I.; et al.: High-performance liquid chromatographic assay of the magnetic resonance imaging contrast agent gadobenate in plasma, urine and bile. *Journal of Chromatography B: Biomedical Sciences and Applications*. 1994, **656**(2), 415-422. DOI: 10.1016/0378-4347(94)80099-5. ISSN 03784347.

[98] MAZZUCOTELLI, A.; BAVASTELLO, V.; et al.: Analysis of gadolinium polyaminopolycarboxylic complexes by HPLC–ultrasonic nebulizer–ICP-AES hyphenated technique. *Anal. Proc*. 1995, **32**(5), 165-167. DOI: 10.1039/AI9953200165. ISSN 0144-557x.

[99] MÖLLER, P.; DULSKI, P.; BAU, M.; et al.: Anthropogenic gadolinium as a conservative tracer in hydrology. *Journal of Geochemical Exploration*. 2000, **69-70**, 409-414. DOI: 10.1016/S0375-6742(00)00083-2. ISSN 03756742.

[100] MOUTIEZ, E.; PROGNON, P.; MAHUZIER, G.; et al.: Time-resolved Luminescence as a Novel Detection Mode for the Simultaneous High-performance Liquid Chromatographic Determination of Gadolinium–DOTA and Gd3+. *The Analyst*. **122**(11), 1347-1352. DOI: 10.1039/a703800c. ISSN 00032654.

[101] NORMANN, P.T.; HALS, P.A.: In vivo stability and excretion of gadodiamide (GdDTPA-BMA), a hydrophilic gadolinium complex used as a contrast enhancing agent for magnetic resonance imaging. *European Journal of Grug Metabolism and Pharmacokinetics.* 1995, **20**(4), 307-313.

[102] NOZAKI, Y.; LERCHE, D.; ALIBO, D.S.; TSUTSUMI, M.: Dissolved indium and rare earth elements in three Japanese rivers and Tokyo Bay: Evidence for anthropogenic Gd and In. *Geochimica et Cosmochimica Acta*. 2000, **64**(23), 3975-3982. DOI: 10.1016/S0016-7037(00)00472-5. ISSN 00167037.

[103] OKADA, S.; KATAGIRI, K.; et al.: Safety of Gadolinium Contrast Agent in Hemodialysis Patients. *Acta Radiologica*. 2001, **42**(3), 339-341. DOI: 10.1080/028418501127346756. ISSN 0284-1851.

[104] PUTTAGUNTA, N.; WENDELL, R.; et al.: Comparative Transmetallation Kinetics and Thermodynamic Stability of Gadolinium-DTPA Bis-Glucosamide and Other Magnetic Resonance Imaging Contrast Media. *Investigative Radiology*. 1996,**31**(10), 619-624. DOI: 10.1097/00004424-199610000-00003. ISSN 0020-9996.

[105] RAJU, K.C.S.; COSSMER, A.; SCHARF, H.; et al.: Speciation of gadolinium based MRI contrast agents in environmental water samples using hydrophilic interaction chromatography hyphenated with inductively coupled plasma mass spectrometry. *J. Anal. At. Spectrom*. 2010, **25**(1), 55-61. DOI: 10.1039/B919959D. ISSN 0267-9477.

[106] SAUSSEREAU, E.; LACROIX, C.; CATTANEO, A.; et al.: Hair and fingernail gadolinium ICP-MS contents in an overdose case associated with nephrogenic systemic fibrosis. *Forensic Science International*. 2008, **176**(1), 54-57. DOI: 10.1016/j.forsciint.2007.06.026. ISSN 03790738.

[107] SCHUHMANN-GIAMPIERI, G.; KRESTIN, G.: Pharmacokinetics of Gd-DTPA in Patients with Chronic Renal Failure.*Investigative Radiology*. 1991, **26**(11), 975-979. DOI: 10.1097/00004424-199111000-00009. ISSN 0020-9996.

[108] TELGMANN, L.; HOLTKAMP, M.; KÜNNEMEYER, J.; et al.: Simple and rapid quantification of gadolinium in urine and blood plasma samples by means of total reflection X-ray fluorescence (TXRF). *Metallomics*. 2011, **3**(10), 1035-1040. DOI: 10.1039/c1mt00054c. ISSN 1756-5901.

[109] TELGMANN, L.; WEHE, CH.; KÜNNEMEYER, J.; et al.: Speciation of Gd-based MRI contrast agents and potential products of transmetalation with iron ions or parenteral iron supplements. *Analytical and Bioanalytical Chemistry*. 2012, **404**(8), 2133-2141. DOI: 10.1007/s00216-012-6404-x. ISSN 1618-2642.

[110] TELGMANN, L.; WEHE, CH.; BIRKA, M.; et al.: Speciation and Isotope Dilution Analysis of Gadolinium-Based Contrast Agents in Wastewater. *Environmental Science & Technology*. 2012, **46**(21), 11929-11936. DOI: 10.1021/es301981z. ISSN 0013-936x.

[111] TWEEDLE, M.F.; HAGAN, J.; KUMAR, K.; et al.: Reaction of gadolinium chelates with endogenously available ions.*Magnetic Resonance Imaging*. 1991, **9**(3), 409-415. DOI: 10.1016/0730-725X(91)90429-P. ISSN 0730725x.

[112] VERPLANCK, P.; TAYLOR, L.; et al.: Aqueous Stability of Gadolinium in Surface Waters Receiving Sewage Treatment Plant Effluent, Boulder Creek, Colorado.*Environmental Science & Technology*. 2005, **39**(18), 6923-6929. DOI: 10.1021/es048456u. ISSN 0013-936x.

[113] VORA, M.; WUKOVNIG, S.; FINN, R.; et al.: Reversed-phase high-performance liquid chromatographic determinationof gadolinium-diethylenetriaminepentaacetic acid complex. *Journal of Chromatography A*. 1986, **369**, 187-192. DOI: 10.1016/S0021-9673(00)90114-6. ISSN 00219673.

[114] WEINMANN, H.J.; LANIADO, M.: Pharmacokinetics of GDDTPA dimeglumine after intravenous-injection into healthy-volunteers. *Phusiological Chemistry and Physics and Medical NMR.* 1984, **16**(2), 167-172.

[115] ZHU, Y.; HOSHINO, M.; et al.: Gadolinium Anomaly in the Distributions of Rare Earth Elements Observed for Coastal Seawater and River Waters around Nagoya City. *Bulletin of the Chemical Society of Japan*. 2004, **77**(10), 1835-1842. DOI: 10.1246/bcsj.77.1835. ISSN 0009-2673.

[116] MAHDIEH, M.H.; AKBARI JAFARABADI, M.: Optical characterization of thermal lens effect in ethanol and the influence of focusing lens and liquid cell size. *Optics & Laser Technology* . 2012, **44**(1), 78-82. DOI: 10.1016/j.optlastec.2011.05.023. ISSN 00303992.

[117] TRAN, C.D.; FRANKO, M.: Thermal Lens Spectroscopy. *Encyclopedia of Analytical Chemistry*, eds. R.A. Meyers, John Wiley: Chichester., 2010. DOI: 9780470027318.

[118] FRANKO, M.; TRAN, C.D.: Analytical thermal lens instrumentation. *Review of Scientific Instruments*. 1996, **67**(1), 1-18. DOI: 10.1063/1.1147512. ISSN 00346748.

[119] BIALKOWSKI, S. E.: Photothermal Spectroscopy Methods for Chemical Analysis. *Chemical Analysis*,eds. J.D. Winefordner, John Whiley & Sons, Inc. 1996,134.

[120] SATO, K.; HIBARA, A.; et al.: Microchip-based chemical and biochemical analysis systems. *Advanced Drug Delivery Reviews*. 2003,**55**(3), 379-391. DOI: 10.1016/S0169-409X(02)00225-9. ISSN 0169409x.

[121] FRANKO, M.: Thermal Lens Spectrometric Detection in Flow Injection Analysis and Separation Techniques. *Applied Spectroscopy Reviews*. 2008, **43**(4), 358-388. DOI: 10.1080/05704920802108032. ISSN 0570-4928.

[122] FRANKO, M.: Recent applications of thermal lens spectrometry in food analysis and environmental research. *Talanta*. 2001, **54**(1), 1-13. DOI: 10.1016/S0039-9140(00)00608-1. ISSN 00399140.

[123] POGAČNIK, L.; FRANKO, M.: Detection of organophosphate and carbamate pesticides in vegetable samples by a photothermal biosensor. *Biosensors and Bioelectronics*. 2003, **18**(1), 1-9. DOI: 10.1016/S0956-5663(02)00056-8. ISSN 09565663.

[124] ŠIKOVEC, M.; FRANKO, M.; et.al.: Effect of organic solvents in the on-line thermal lens spectrometric detection of chromium(III) and chromium(VI) after ion chromatographic separation. *Journal of Chromatography A*. 2001, **920**(1-2), 119-125. DOI: 10.1016/S0021-9673(01)00611-2. ISSN 00219673.

[125] SURMEIAN, M.; HIBARA, A.; et al.: Distribution of methyl red on the water‐organic liquid interface in a microchannel. *Analytical Letters*. 2001, **34**(9), 1421-1429. DOI: 10.1081/AL-100104916. ISSN 0003-2719.

[126] LIMA, S.M.; SAMPAIO, J.A.; et al.: Mode-mismatched thermal lens spectrometry for thermo-optical properties measurement in optical glasses: a review.*Journal of Non-Crystalline Solids*. 2000, **273**(1-3), 215-227. DOI: 10.1016/S0022-3093(00)00169-1. ISSN 00223093.

[127] CHANLON, S.; GEORGES, J.: Pulsed-laser mode-mismatched crossed-beam thermal lens spectrometry within a small capillary tube: effect of flow rate and beam offset on the photothermal signal. *Spectrochimica Acta Part A: Molecular and Biomolecular Spectroscopy*. 2002, **58**(8), 1607-1613. DOI: 10.1016/S1386-1425(01)00612-6. ISSN 13861425.

[128] SATO, K.; YAMANAKA, M.; et al.: Microchip-based immunoassay system with branching multichannels for simultaneous determination of interferon-gamma. *Electrophoresis*. 2002, **23**(5), 734-769.

[129] LUTEROTTI, S.; FRANKO, M.; BICANIC, D.: Ultrasensitive determination of β-carotene in fish oil-based supplementary drugs by HPLC-TLS. *Journal of Pharmaceutical and Biomedical Analysis*. 1999, **21**(5), 901-909. DOI: 10.1016/S0731-7085(99)00185-5. ISSN 07317085.

[130] TANAKA, Y.; SLYADNEV, M.; et al.: Non-contact photothermal control of enzyme reactions on a microchip by using a compact diode laser.*Journal of Chromatography A*. 2000, **894**(1-2), 45-51. DOI: 10.1016/S0021-9673(00)00593-8. ISSN 00219673.

[131] POGACNIK, L.; FRANKO, M.: Optimisation of FIA system for detection of organophosphorus and carbamate pesticides based on cholinesterase inhibition. *Talanta*. **54**(4), 631-641. DOI: 10.1016/S0039-9140(01)00314-9. ISSN 00399140.

[132] KIKUTANI, Y.; HISAMOTO, H.; et al.: Micro wet analysis system using multi-phase laminar flows in three-dimensional microchannel networkElectronic supplementary information (ESI) available: illustration and microscopic view of two-phase laminar flow. See http. *Lab on a Chip*. 2004, **4**(4), 328-332. DOI: 10.1039/b400233d. ISSN 1473-0197.

[133] KORTE, D.; BRUZZONITI, M.C.; et al.: Thermal Lens Spectrometric Determination of Colloidal and Ionic Silver in Water. *International Journal of Thermophysics*. 2011, **32**(4), 818-827. DOI: 10.1007/s10765-010-0856-z. ISSN 0195-928x.

[134] MADŽGALJ, A.; BAESSO, M.L.; FRANKO, M.: Flow injection thermal lens spectrometric detection of hexavalent chromium. *The European Physical Journal Special Topics*. 2008, **153**(1), 503-506. DOI: 10.1140/epjst/e2008-00494-4. ISSN 1951-6355.

[135] GHALEB, K.A.; STEPHAN, K.; et al.: Investigation of the Mixing Efficiency of a Chaotic Micromixer Using Thermal Lens Spectrometry. *Applied Spectroscopy*. 2006, **60**(5), 564-567. DOI: 10.1366/000370206777412211. ISSN 00037028.

[136] PROSKURNIN, M. A.; VOLKOV, D.S.; et al.: Advances in thermal lens spectrometry. *Journal of Analytical Chemistry*. 2015, **70**(3), 249-276. DOI: 10.1134/S1061934815030168. ISSN 1061-9348.

[137] YU, F.; KACHANOV, A.; KOULIKOV, S.; et al.: Ultraviolet thermal lensing detection of amino acids. *Journal of Chromatography A*. 2009, **1216**(16), 3423-3430. DOI: 10.1016/j.chroma.2008.05.096. ISSN 00219673.

[138] TOKESHI, M.; KITAMORI, T.: Integrated micro chemical lab: Detection of biomolecules and expectation to electrochemistry. *Electrochemistr.* 2000, **63**(3), 192-196.

[139] XIONG, B.; WANG, W.; et al.: Simultaneous laser-induced fluorescence, coaxial thermal lens spectroscopy and retro-reflected beam interference detection for capillary electrophoresis. *Talanta*. 2012, **88**, 168-174. DOI: 10.1016/j.talanta.2011.10.027. ISSN 00399140.

[140] XIONG, B.; MIAO, X.; et al.: Simultaneous coaxial thermal lens spectroscopy and retro-reflected beam interference detection for capillary electrophoresis. *Journal of Chromatography A*. 2008, **1209**(1-2), 260-266. DOI: 10.1016/j.chroma.2008.09.042. ISSN 00219673.

[141] NEDOSEKIN, D.A.; BENDRYSHEVA, S.N.; et al.: Indirect thermal lens detection for capillary electrophoresis. *Talanta*. 2007, **71**(4), 1788-1794. DOI: 10.1016/j.talanta.2006.08.016. ISSN 00399140.

[142] XIONG, B.; WANG, W.; et al.: Simultaneous laser-induced fluorescence, coaxial thermal lens spectroscopy and retro-reflected beam interference detection for capillary electrophoresis. *Talanta*. 2012, **88**, 168-174. DOI: 10.1016/j.talanta.2011.10.027. ISSN 00399140.

[143] PROSKURNIN, M.A.; SLYADNEV, M.; et al.: Optimisation of thermal lens microscopic measurements in a microchip. *Analytica Chimica Acta*. 2003,**480**(1), 79-95. DOI: 10.1016/S0003-2670(02)01546-5. ISSN 00032670.

[145] UCHIYAMA, K.; HIBARA, A.; et al.: An interface chip connection between capillary electrophoresis and thermal lens microscope.*ELECTROPHORESIS*. **24**(12), 179-184. DOI: 10.1002/elps.200390011. ISSN 01730835.

[146] SURMEIAN, M.; SLYADNEV, M.N.; et al.: Three-layer flow membrane system on a microchip for investigation of molecular transport.*Analytical Chemistry*. 2002, **74**(9), 2014-2020.

[147] TAMAKI, E.; HIBARA, A.; et al.: Microchannel-assisted thermal-lens spectrometry for microchip analysis. *Journal of Chromatography A*. 2003,**987**(1-2), 197-204. DOI: 10.1016/S0021-9673(02)01661-8. ISSN 00219673.

[148] SMIRNOVA, A.; MAWATARI, K.; et al.: Micro-multiphase laminar flows for the extraction and detection of carbaryl derivative. *Analytica Chimica Acta* . 2006, **558**(1-2), 69-74. DOI: 10.1016/j.aca.2005.10.073. ISSN 00032670.

[149] HISAMOTO, H.; HORIUCHI, T.; et al.: On-Chip Integration of Neutral Ionophore-Based Ion Pair Extraction Reaction. *Analytical Chemistry*. 2001, **73**(6), 1382-1386. DOI: 10.1021/ac001271v. ISSN 0003-2700.

[150] HIBARA, A.; NONAKA, M.; et al.: Spectroscopic Analysis of Liquid/Liquid Interfaces in Multiphase Microflows. *Journal of the American Chemical Society*. 2003, **125**(49), 14954-14955. DOI: 10.1021/ja037308l. ISSN 0002-7863.

[151] ŠULIGOJ, A.; CERNIGOJ, U.; ŠTANGAR, L.U.: Preparation procedure of durable titania coatings on metal supports for photocatalytic cleaning applications. 2010, Patent number SI 23585 A: The Slovenian Intellectual Property Office, Ljubljana.

[152] BIRKA, M.; ROSCHER, J.; et al.: Investigating the stability of gadolinium based contrast agents towards UV radiation. *Water Research* . 2016, **91**, 244-250. DOI: 10.1016/j.watres.2016.01.012. ISSN 00431354.

[153] CYRIS, M.; KNOLLE, W.; et al.: Reaction of Gadolinium Chelates with Ozone and Hydroxyl Radicals.*Environmental Science & Technology*. 2013, **47**(17), 9942-9949. DOI: 10.1021/es402219u. ISSN 0013-936x.

[154] COWPER, S.E.; SU, L.D.; et al.: Nephrogenic Fibrosing Dermopathy. *The American Journal of Dermatopathology*. 2001, **23**(5), 383-393. DOI: 10.1097/00000372-200110000-00001. ISSN 0193-1091.

[155] GALAN, A.; COWPER, S.E.; BUCALA, R.: Nephrogenic systemic fibrosis (nephrogenic fibrosing dermopathy). *Current Opinion in Rheumatology*. 2006, **18**(6), 614-617. DOI: 10.1097/01.bor.0000245725.94887.8d. ISSN 1040-8711.

[156] COWPER, S.E.: Nephrogenic Systemic Fibrosis: The Nosological and Conceptual Evolution of Nephrogenic Fibrosing Dermopathy.*American Journal of Kidney Diseases*. 2005, **46**(4), 763-765. DOI: 10.1053/j.ajkd.2005.08.008. ISSN 02726386.

[157] MARCKMANN, P.: Nephrogenic Systemic Fibrosis: Suspected Causative Role of Gadodiamide Used for Contrast-Enhanced Magnetic Resonance Imaging. *Journal of the American Society of Nephrology*. 2006, **17**(9), 2359-2362. DOI: 10.1681/ASN.2006060601. ISSN 1046-6673.

[158] CARAVAN, P.; ELLISON, J.J.; et al.: Gadolinium(III) Chealates as MRI Contrast Agents: Structure, Dynamics, and Applications.*Chem. Rev.*1999, **99**, 2293-2352.

[159] CHENG, K.T.; Gadobutrol, *Molecular Imaging and Contrast Agent Database (MICAD)* [Internet], http://www.ncbi.nlm.nih.gov/books/NBK23589/

[160] MATHEW, A.; KUMAR, AVK.; et al.: Spectrophotometric determination of Neodynium(III), Samarium(III), Gadolinium(III), Terbium(III), Dysprosium(III), Holmium(III) in micellar media. *Indian Journal of Chemical Technology*. 2012, 19(5), 331-336.

[161] LIU, M.; FRANKO, M.: Thermal lens spectrometry under excitation of a divergent pump beam. *Applied Physics B*. 2014, **115**(2), 269-277. DOI: 10.1007/s00340-013-5601-4. ISSN 0946-2171.

[162] Effects on Biotic System. *OECD Guidelines for the Testing of Chemicals: Section 2*. ISBN 9789264022386. Available at: http://www.oecd-ilibrary.org/environment/summary-of-considerations-in-the-report-from-the-oecd-expert-group-on-ecotoxicology_9789264022386-en

[163] PETRUCCI, Ralph H. *General chemistry: principles and modern applications*. 9th ed. Upper Saddle River, N.J.: Pearson/Prentice Hall, c2007. ISBN 9780131493308.

[164] ATKINS, P. W. a Julio. DE PAULA. *Physical chemistry for the life sciences*. 2nd ed. Oxford: Oxford University Press, 2011. ISBN 0199564280.

9. ABBREVIATIONS

AOP	advanced oxidation processes
BGE	background electrolyte
CA	contrast agent(s)
CAS	chemical abstracts service registry number
CE	capillary electrophoresis
CTAB	hexadecyltrimethylammonium bromide
e.g.	exempli gratia (for example)
em.	emission wavelength
ESI	electrospray ionization
ex.	excitation wavelength
FIA	flow injection analysis
HILIC	hydrophilic interaction chromatography
HPLC	high performance liquid chromatography
IC	ion chromatography
ICP	inductively coupled plasma
i.e.	id est (that is/namely)
λ	wavelength
LOD	limit of detection
LOQ	limit of quantification
MB	methylene blue
MP	mobile phase
MRI	magnetic resonace imaging
MS	mass spectrometry
NFD	nephrogenic fibrosing dermopathy
NPOC	non-purgeable organic carbon
NSF	nephrogenic system fibrosis
OECD	Organisation for Economic Co-operation and Development
OES	optical emission spectrometry
PAN	1-(2-Pyridylazo)-2-naphtol
Rad.	radioactivity detection
RE	reference electrode material
REE	rare earth elements
SEM	scanning electron microscope
SF	double focusing magnetic sector field
SIMS	secondary ion mass spectrometry
T_1	longitudinal relaxation rate
T_2	transverse relaxation rate
TLM	thermal lens microcsope
TLS	thermal lens spectrometry
TN	total nitrogen
TOC	total organic carbon
TXRF	total X-ray fluorescence spectroscopy
UV	ultraviolet light
UV-Vis	ultraviolet and visible light spectrophotomoetry
VUV	vacuum ultraviolet
WE	working electrode material
WWTP	wastewater treatment plant
YAG	yttrium aluminium garnet

10. ATTACHMENTS

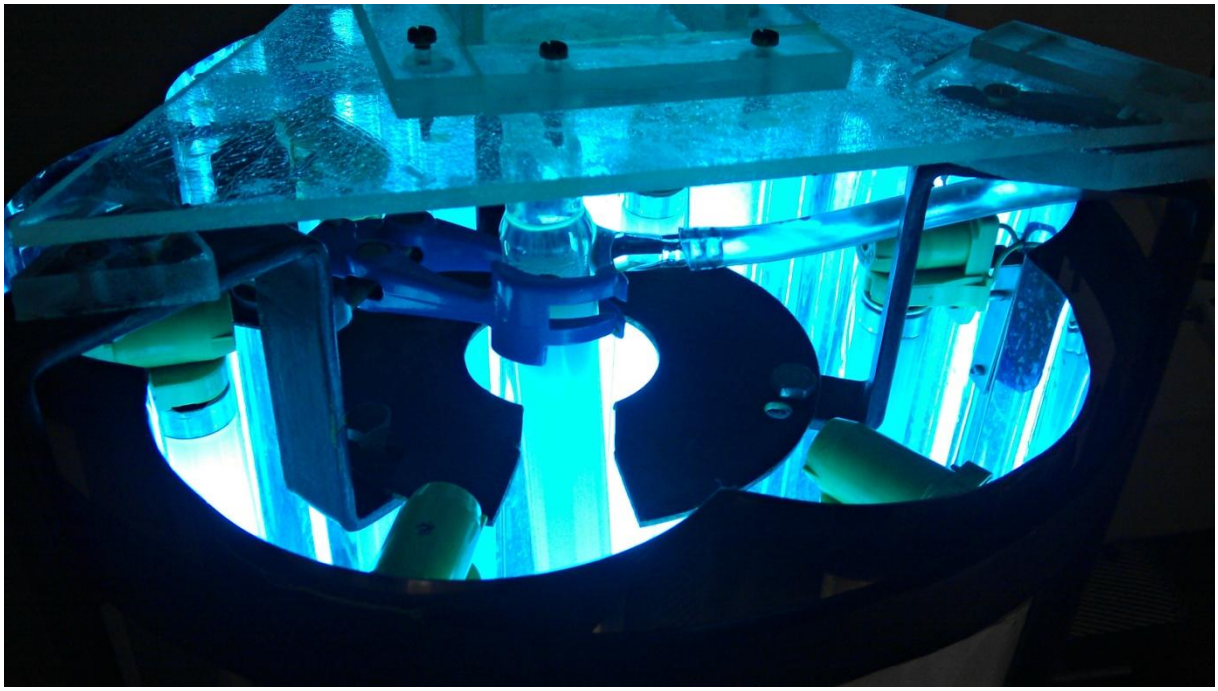

Figure 32. Reactor cell with TiO_2 suspension inside the reactor

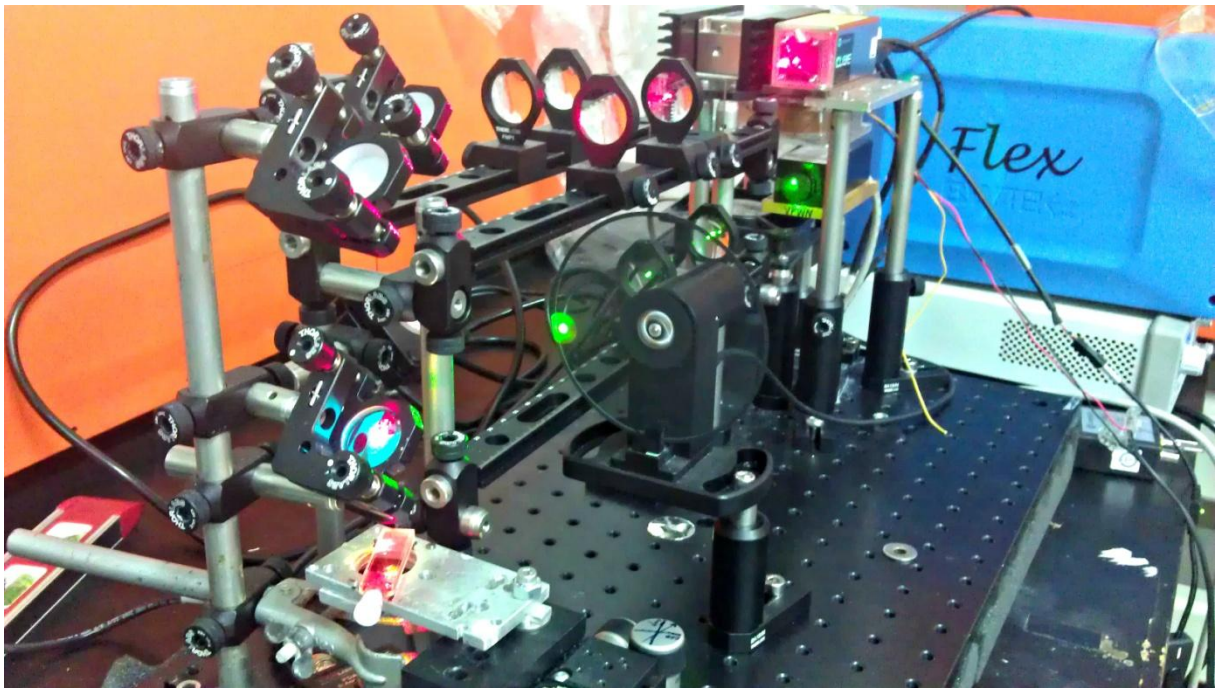

Figure 33. TLM system

Figure 34. Reaction cell with TiO_2 slide in it.

Figure 35. TOC/TN analyzer, AG MULTI N/C 3100, Analytik Jena